NASA Technical Memorandum 102781

A Finite Reynolds Number Approach for the Prediction of Boundary Layer Receptivity in Localized Regions

Meelan Choudhari
Craig L. Streett

January 1991

National Aeronautics and Space Administration

Langley Research Center
Hampton, Virginia 23665

A Finite Reynolds Number Approach for the Prediction of Boundary Layer Receptivity in Localized Regions

Meelan Choudhari
High Technology Corporation
Hampton, VA 23666

Craig L. Streett
NASA Langley Research Center
Hampton, VA 23665

Abstract

Previous theoretical work on the boundary layer receptivity problem has utilized large Reynolds number asymptotic theories, thus being limited to a narrow part of the frequency - Reynolds number domain. We present an alternative approach for the prediction of localized instability generation which has a general applicability, and also accounts for finite Reynolds number effects. This approach is illustrated for the case of Tollmien-Schlichting wave generation in a Blasius boundary layer due to the interaction of a free-stream acoustic wave with a region of short-scale variation in the surface boundary condition. The specific types of wall inhomogeneities examined are: regions of short scale variations in wall suction, wall admittance and wall geometry (roughness). Extensive comparison is made between the results of the finite Reynolds number approach and previous asymptotic predictions. This comparison also suggests an alternative way of utilizing the latter at Reynolds numbers of interest in practice.

1. INTRODUCTION

Laminar-turbulent transition is a result of instability of the laminar state. At high Reynolds numbers, suitable perturbations to this state are amplified, eventually leading to the stable (in-the-large) turbulent state. It is important to note that the introduction of these "suitable" perturbations (i.e., instabilities) into the boundary layer flow is a necessary prerequisite for transition to occur. The process by which the boundary layer internalizes the external disturbances in the form of instability waves is known as the boundary layer receptivity. Once generated, these instability waves undergo linear amplification and nonlinear interactions before the flow becomes fully turbulent.

Therefore, receptivity signifies the genesis of boundary layer transition. Goldstein[1,2], Ruban[3] and Goldstein *et al*[4] utilized high Reynolds number asymptotic methods

to elucidate the basic mechanisms responsible for making the boundary layer "receptive" to external disturbances. This pioneering work provided much of the impetus for further work in receptivity during the past few years. In the remainder of this section, we first briefly describe the general features of Goldstein's receptivity theory. Following this, we summarize the receptivity research that followed Goldstein's work, and present the problem addressed in this paper.

The classical linear stability theory is based upon the disparity between the streamwise length-scales of the instability motion and the mean boundary layer. The instability waves correspond to the short-scale, nearly periodic eigensolutions of the slowly developing boundary layer which have a small growth rate for parameter values between the neutral boundaries. The obvious implication of the locally periodic nature of the instability wave is that the wave is decoupled from any other spatially periodic motion with a different wavelength.

It is obvious that in order to generate an instability wave of a particular frequency, one would require a forcing which has not only the same frequency, but also a spatial scale that matches the instability wavelength. However, free-stream disturbances are governed by the inviscid dynamics outside the boundary layer, while the instability waves represent free oscillations (or eigenmodes) of the flow within the boundary layer. Hence, the wavelengths of these two types of disturbances are, in general, quite different. In fact, in low-speed flows, the free-stream disturbances (which can either be acoustic waves or convected vorticity disturbances, i.e., free-stream turbulence) have wavelengths which are much longer than the instability wavelengths. The free-stream unsteadiness can then be "tuned" to the instability length-scale only through an interaction with the spatial spectrum of the mean boundary layer.

Since a slowly developing (or "quasi-parallel") mean boundary layer does not have the short length-scales required for the tuning process, receptivity will usually occur only in regions of non-parallel mean flow. Goldstein showed that there are two classes of regions where the mean flow becomes non-parallel. The first class of non-parallel mean flow regions corresponds to the region close to the leading edge, where the boundary layer thickness is changing rapidly. The second category, which is much more diverse, involves regions farther downstream of the leading edge. Here the mean-flow becomes non-parallel due to either a short-scale variation in the surface boundary condition or an adverse pressure gradient provoking a separation of the mean boundary layer. The short-scale variations in surface boundary condition correspond to changes in surface geometry (wall roughness), wall suction/blowing velocity or wall temperature. The latter two cases are especially relevant to laminar flow control (LFC) where suction and heating (water) or cooling (air) are utilized for stabilizing the boundary layer. The variations in boundary conditions can be either local (isolated roughness elements, well-separated suction/heating strips) or

distributed over a large number of instability wavelengths (distributed roughness, surface waviness, closely spaced suction/heating strips); however, the role of the short-scale variation is the same in both cases, viz., to provide the tuning required for producing the appropriate forcing.

In comparing the two classes of receptivity regions, it is important to note that instability waves generated near the leading edge undergo an exponential decay upstream of the lower branch neutral stability point, even a weak receptivity mechanism close to the neutral point is likely to be more important than a much stronger receptivity mechanism near the leading edge[5]. In practice, the exponential decay between the leading edge and the neutral stability point is decreased somewhat due to the presence of an adverse pressure gradient region close to the leading edge. However, in this paper we concentrate on the second class of receptivity regions.

Goldstein[2] and Ruban[3] presented analytical solutions for the specific case of receptivity due to the interaction of a free-stream acoustic wave with a small but sudden variation in the surface geometry. Their analysis was limited to two-dimensional flows in terms of both the mean boundary layer as well as the instability wave generated due to the interaction. However, the asymptotic framework of Goldstein and Ruban was later extended by other investigators to a variety of other problems in the second class of non-parallel mean flow regions. Bodonyi *et al*[6] considered the case where the mean flow perturbation due to the wall hump is not small enough to permit linearization with respect to the oncoming boundary layer. Choudhari[5] analyzed receptivity mechanisms arising in LFC applications which employ suction through a porous surface as a means of stabilizing the boundary layer. He showed that in addition to the receptivity caused by mean flow gradients due to variations in the wall suction distribution, the short-scale variation in the admittance of the porous surface directly scatters energy from the acoustic wave to the instability wave. The latter mechanism is operational even in the absence of a mean flow adjustment. Choudhari and Kerschen[7] studied the three-dimensional interaction of a free-stream acoustic wave with a wall inhomogeneity of above types which has short-scale variations in both the streamwise and spanwise directions. Kerschen[8] and Choudhari and Kerschen[9] investigated the generation of instability waves near a wall hump due to a convected vorticity disturbance in the free stream. Finally, localized generation of T-S waves in two and three-dimensional supersonic boundary layers was analyzed by the present authors[10] in the context of two and three-dimensional supersonic boundary layers.

All previous investigations discussed above utilized the asymptotic (triple deck) framework. Although useful in their own right, these predictions were based on a single-term asymptotic expansion. However, the critical receptivity region corresponds to locations upstream of or close to the lower branch of the neutral stability curve, i.e., Reynolds numbers smaller than those in the main part of the

unstable regime, where the quantitative accuracy of the asymptotic predictions is questionable. In this paper, we present an alternative approach for the prediction of receptivity in localized regions which would yield relatively accurate results in the Reynolds-number-range of interest in practice. For simplicity, attention is restricted to the case of incompressible flows over two-dimensional airfoils. However, the present approach also provides a viable framework for the prediction of localized receptivity in such complex flows as compressible and three-dimensional boundary layers. In section 2, we formulate the problem for the local interaction of a free-stream acoustic wave with an arbitrary wall inhomogeneity. It is shown that the local receptivity problem reduces to an inhomogeneous Orr-Sommerfeld (henceforth O-S) problem in the Fourier transform space, and the amplitude of the generated instability wave can be determined as the residue of the pole corresponding to that particular eigenvalue of the O-S problem which represents the wavenumber of the Tollmien-Schlichting (T-S) instability wave. In section 3, we present results which show the variation of the receptivity coefficient in the frequency parameter - Reynolds number space. Detailed comparison of these results with the asymptotic predictions is also presented in Section 3. Although the discussion in this paper pertains only to localized inhomogeneities, in section 4, we also point out the possible application of this analysis to distributed regions of short-scale variations. In addition to accounting for the finite Reynolds number effects, the present approach has other advantages over the asymptotic theory, and these are discussed in Section 5.

2. ANALYSIS

This section provides a summary of the finite Reynolds number approach. In order to assess the finite Reynolds number effects on localized receptivity mechanisms in the simplest possible setting, we focus attention on a two-dimensional, incompressible flow past a semi-infinite, flat-plate airfoil. However, the present approach can easily be applied to other types of geometries as well. The free-stream speed, density and kinematic viscosity corresponding to the oncoming flow are denoted by U^*_∞, ρ^* and ν^*, respectively. The unsteady free-stream disturbance is assumed to be a plane, harmonic acoustic wave propagating parallel to the plate in the downstream direction. Since the acoustic wavelength is infinite in the zero Mach number limit, the free-stream flow consists of a uniform flow with mean velocity U^*_∞ plus a harmonic perturbation of amplitude u^*_{ac} and frequency ω^*. The uniform velocity fluctuation u^*_{ac} is also accompanied by a uniform, time harmonic pressure gradient with an amplitude $i\omega^* u^*_{ac}$. We assume the nondimensional amplitude of the free-stream fluctuation to be sufficiently small ($\epsilon_{fs} = u^*_{ac}/U^*_\infty << 1$) so that the unsteady motion can be treated as a small perturbation of the local mean flow.

The receptivity is assumed to occur due to a localized wall inhomogeneity involving a variation in one or more of the surface boundary conditions. Some remarks concerning the application of results for the localized case to an extended region of receptivity are presented in Section 4. We assume that the distribution of the normal component of the steady or unsteady velocity at the wall, or the wall height distribution has a short-scale variation with respect to the streamwise coordinate in a local region which is a distance ℓ^* from the leading edge (Figs. 1a-1c and Fig. 2). While the nonzero mean normal velocity represents the wall suction/blowing distribution, the short-scale distribution of the unsteady normal velocity at the wall has been introduced in order to model the effects of rapidly varying surface admittance in an incompressible flow.

The admittance of a surface is defined as the ratio, at the surface, of the unsteady normal velocity to the fluctuating component of pressure. Since the absolute value of the pressure becomes irrelevant in the incompressible limit, we specify the distribution of the unsteady normal velocity at the wall instead of directly imposing a short-scale distribution of the wall admittance. Even in the compressible case analyzed by Choudhari[5] using asymptotic theory, the mathematical statement of the inhomogeneous boundary condition reduces to the specification of the unsteady normal velocity at the wall. Therefore, the present treatment of the wall admittance variation poses little difficulty in the comparison of present results with the asymptotic predictions. It is worth noting that in addition to modelling the wall admittance variation, the unsteady mass flux at the wall may also represent unsteady disturbances within the suction system, especially the designs with large suction slots.

The maximum amplitudes of the local variations in different types of wall boundary conditions (as described above) are denoted by the nondimensional parameters $\epsilon_w^{(j)}$, where the index j varies from one to three depending on the type of wall inhomogeneity. Specifically, the parameter $\epsilon_w^{(1)}$ corresponds to the normalized wall suction/blowing velocity, V_w^*/U_∞^*, while $\epsilon_w^{(2)}$ denotes v_w^*/u_{ac}^*, the unsteady vertical velocity at the porous surface normalized by the free-stream disturbance velocity. The parameter $\epsilon_w^{(2)}$ can be related to the amplitude of the wall-admittance variation, $\beta_w^* \rho^* U_\infty^*$, where β_w^* denotes the wall admittance as defined in the preceding paragraph. Finally, $\epsilon_w^{(3)}$ denotes the roughness height, H_w^*/δ^*, where δ^* is the displacement thickness of the Blasius boundary layer at the location of the wall inhomogeneity (i.e., the mean flow in the absence of any localized variations). All three parameters $\epsilon_w^{(j)}$, are assumed to be small enough to allow linear analyses of the different mechanisms and superposition of the results. While the assumed orders of magnitudes for the wall-suction and wall-admittance are consistent with typical parameter values in LFC systems, the roughness heights can vary over a wide range in practice. The assumption of small roughness height allows us to compare results

with the asymptotic predictions of Goldstein[2].

Since the roughness element and the variation in wall suction are assumed to produce only a small perturbation to the Blasius boundary layer the stability properties of the perturbed mean flow (i.e., the mean flow in presence of the perturbation due to the wall suction or wall geometry variation) are identical to those of the Blasius boundary layer, to the leading order. We assume the Reynolds number $R_{\delta^*} = U^*_\infty \delta^* / \nu^*$, based upon the local displacement thickness of the unperturbed mean boundary layer, to be large enough such that the stability of the unperturbed mean flow at the location of the wall inhomogeneity is governed by the classical, quasi-parallel stability theory. Strictly speaking, the large Reynolds number assumption is inherent within the boundary layer approximation for the mean flow. In practice, however, the quasi-parallel stability theory has been found to be reasonable only for Reynolds numbers much larger than those at which the mean flow is accurately described by the boundary layer theory. For the Blasius boundary layer, this constraint (approximately) corresponds to Reynolds numbers larger than the minimum critical Reynolds number of 520.

We further assume that the length-scale of the local variations, L^*, is of the same order as the local T-S wavelength. This provides the necessary ingredient for the wavelength reduction from the free-stream disturbance to the instability wave. In this paper we restrict attention to a localized region of receptivity. However, remarks concerning the extension of these results to distributed regions of receptivity will also be presented in Section 4.

Since the instability wavelength is much shorter than the length-scale of the mean boundary layer (i.e., $\epsilon_\ell = L^*/\ell^* << 1$), we can utilize the method of matched asymptotic expansions to simplify the problem. Thus, we match a local approximation valid in the region of receptivity to an outer (or "global") solution valid farther downstream. The governing equations in the outer region are homogeneous; hence the far downstream solution for the short-scale, unsteady motion produced by the interaction of the free-stream disturbance with the wall inhomogeneity corresponds to a superposition of the discrete and continuous spectrum type eigenmodes in a slowly developing boundary layer. The amplitudes of these eigensolutions are determined by a matching with the solution in the region of receptivity which is the focus of this paper.

We introduce a Cartesian coordinate system $\{x^*, y^*\}$ centered at an arbitrary point within this localized region (Fig. 2). Since we are considering the two-dimensional case, it seems appropriate to simplify the formulation by having the streamfunction as the only dependent variable. The streamfunction ψ is normalized by $U^*_\infty \delta^*$, and we define the local coordinates in the streamwise and transverse directions as $X = x^*/\delta^*$ and $Y = y^*/\delta^*$, respectively. Although for very large Reynolds numbers,

the instability wavelength L^* is of the order of several displacement thicknesses, the choice of δ^* as the local length-scale is motivated by convenience. The slow streamwise coordinate representing the growth of the Blasius boundary layer is defined as $x = x^*/\ell^*$. The nondimensional time t and frequency ω are assumed to have been normalized by δ^*/U^*_∞ and its inverse, respectively.

The streamfunction within the local region, $\psi^{(j)}$, satisfies the two-dimensional Navier-Stokes equation,

$$\frac{\partial \nabla^2 \psi^{(j)}}{\partial t} + \frac{\partial \psi^{(j)}}{\partial Y}\frac{\partial \nabla^2 \psi^{(j)}}{\partial X} - \frac{\partial \psi^{(j)}}{\partial Y^3}\frac{\partial \psi^{(j)}}{\partial X} - \frac{1}{R_{\delta^*}}\nabla^4 \psi^{(j)} = 0 \ , \qquad (2.1)$$

where j=1 corresponds to the case of receptivity due to wall suction variation, j=2 to the wall admittance problem while j=3 corresponds to the wall hump case. Streamfunctions $\psi^{(1)}$ and $\psi^{(2)}$ satisfy the inhomogeneous wall boundary conditions

$$\frac{\partial \psi^{(1)}(X,0)}{\partial X} = \epsilon_w^{(1)} F^{(1)}(X) \ , \qquad (2.2a)$$

and

$$\frac{\partial \psi^{(2)}(X,0)}{\partial X} = \epsilon_{fs}\epsilon_w^{(2)} F^{(2)}(X)\, e^{-i\omega t} \ , \qquad (2.2b)$$

corresponding to specified distributions of the mean and unsteady components, respectively, of the normal velocity at the wall. In addition, $\psi^{(1)}$ and $\psi^{(2)}$ must satisfy the no-slip boundary condition

$$\frac{\partial \psi^{(j)}(X,0)}{\partial Y} = 0 \ , \ j = 1,2 \ . \qquad (2.2c,d)$$

On the other hand, $\psi^{(3)}$ satisfies the impermeability as well as the no-slip boundary condition at the deformed surface location,

$$\psi^{(3)} = \frac{\partial \psi^{(3)}}{\partial Y} = 0 \quad \text{at} \quad Y_w = \epsilon_w^{(3)} F^{(3)}(X) \ . \qquad (2.3a,b)$$

The functions $F^{(j)}(X)$ $(j = 1-3)$ denoting the normalized spatial distributions of the wall inhomogeneities are assumed to be arbitrary throughout the analysis. Finally, we require that all flow quantities approach the respective free-stream values far away from the wall. This implies

$$\psi^{(j)} \to (1 + \epsilon_{fs} e^{-i\omega t})\, Y \ \text{ as } \ Y \to \infty \qquad (2.4)$$

One may observe that four small parameters appear in the problems defined by equations (2.1)-(2.4), namely, $R_{\delta^*}^{-1}, \epsilon_l, \epsilon_{fs}$ and $\epsilon_w^{(j)}$. If one is interested in only a

narrow range of the frequency parameter ω, say in vicinity of one of the two neutral branches, then the two parameters $R_{\delta^*}^{-1}$ and ϵ_l are related to each other for sufficiently large values of the Reynolds number. Similarly, there are restrictions on the wall inhomogeneity amplitudes $\epsilon_w^{(j)}$ in terms of Reynolds number scaling in order that the disturbance produced due to the wall inhomogeneity is a linear perturbation of the base flow. However, in the interest of having a general approach for localized receptivity problems, we treat these parameters as independent of each other. It will be seen from the following analysis that treating these parameters as independent does not affect the amplitude of the generated instability wave.

Hence, we expand the streamfunction within the local region as

$$\psi^{(j)} = \Psi_0(x,Y) \; + \; \epsilon_{fs}\psi_0(x,Y)e^{-i\omega t} \; + \; \epsilon_w^{(j)}\Psi_1^{(j)}(X,Y)$$

$$+\epsilon_{fs}\epsilon_w^{(j)}\psi_1^{(j)}(X,Y)e^{-i\omega t} + O(\epsilon_{fs}^2, {\epsilon_w^{(j)}}^2, \epsilon_l, R_{\delta^*}^{-1}) \;\; , \qquad (2.5)$$

where the upper and lower case variables correspond to the steady and unsteady terms, respectively. The subscript 0 denotes the base flow quantities, i.e., flow within the local region in the absence of any short-scale variation, while the subscript 1 represents the short-scale perturbations to this base flow due to the local wall inhomogeneity. Thus, $\Psi_0(x,Y)$ corresponds to the Blasius streamfunction, while the term involving $\psi_0(x,Y)$ represents the forced signature of the unsteady free-stream disturbance within the Blasius boundary layer. The quantities $\Psi_1^{(1)}(X,Y)$ and $\Psi_1^{(3)}(X,Y)$ correspond to the short-scale mean flow perturbations due to local variations in the wall-suction and wall-height distributions, respectively. Similarly, the term involving $\psi_1^{(j)}(X,Y)$ represents the short-scale corrections to the unsteady signature $\psi_0(x,Y)$ due to the local inhomogeneity. Specifically, $\psi_1^{(1)}$ and $\psi_1^{(3)}$ denote the leading order corrections due to interaction of the basic unsteady solution, ψ_0, with the short-scale mean-flow perturbations corresponding to $\Psi_1^{(1)}$ and $\Psi_1^{(3)}$, respectively. On the other hand, the motion corresponding to $\psi_1^{(2)}$ is induced directly due to the short-scale variation in the unsteady wall-flux. Thus, in each case, ψ_1 denotes the leading order solution for the short-scale, unsteady motion which contains both temporal as well as spatial scales matching those of the instability wave.

The unsteady perturbation ψ_0 to the Blasius boundary layer due to a small amplitude, time harmonic perturbation to the uniform free-stream was investigated by Lighthill[11], and later by Ackerberg and Phillips[12] and Goldstein[1]. Ackerberg and Phillips analyzed the unsteady motion in the "leading edge region" corresponding to distances of the order of a convective wavelength downstream of the leading edge, i.e., $x_1 \equiv \omega^*(\ell^* + x^*)/U_\infty^* = O(1)$. They showed that for $\epsilon' \equiv (\frac{\omega^* \nu^*}{U_\infty^{*2}})^{1/6} << 1$,

the unsteady motion in this region is governed by the linearized unsteady boundary layer equations. Because of the parabolic nature of these equations, the far downstream limit ($x_1 >> 1$) of ψ_0 corresponds to a particular solution ψ_{0p} which exhibits a two layer structure in the transverse direction. Ackerberg and Phillips developed a composite expansion for ψ_{0p} which is valid to $O(x_1)^{-3/2}$ in both these layers.

$$\psi_{0p} = \int_0^Y u_{0p}\, dY\,, \tag{2.6a}$$

where

$$u_{0p} = 1 - e^{i^{3/2}\sigma} - \frac{1}{2ix_1}\eta F'_{Bl}(\eta)$$

$$- \frac{iF''_{Bl}(0)e^{i^{3/2}\sigma}}{2^{5/2}x_1^{3/2}}\left(\frac{3}{2}\sigma + \frac{3}{2\sqrt{i}}\sigma^2 + \frac{i}{3}\right)\sigma^3 \;+\; O\left(\frac{1}{x_1^3}\right). \tag{2.6b}$$

Here σ and η denote the Stokes layer coordinate $\sqrt{\omega R_{\delta^*}}\,Y$, and the Blasius variable $(\delta^*\sqrt{Re_{\ell^*}}/\ell^*)Y$, respectively. Thus, to the leading order, ψ_{0p} is independent of the streamwise coordinate as well as the mean flow, being identical to the Stokes shear wave solution for a purely oscillating flow over an infinite flat plate. Ackerberg and Phillips solved the linearized unsteady boundary layer equations numerically to demonstrate that the unsteady solution approaches the far downstream behaviour through damped oscillations corresponding to the eigensolutions of the linearized unsteady boundary layer equations first found by Lam and Rott[13].

Goldstein[1] analyzed the unsteady motion in the region farther downstream ($x_1 = O(\epsilon'^{-2})$), where the unsteady motion satisfies the Orr-Sommerfeld equation with slowly varying coefficients. This is also the region of interest in this paper since we assumed the wall inhomogeneity to be located in a region where the quasi-parallel stability theory is valid. Goldstein showed that the particular solution (2.6a) is also valid in the Orr-Sommerfeld region. However, the Lam and Rott eigensolutions now match onto the discrete spectrum of the Orr-Sommerfeld equation, the first mode from which corresponds to the Tollmien-Schlichting (T-S) instability wave. This is precisely how an instability wave is generated by the leading edge receptivity mechanism alluded to in the introduction. Upstream of the location correponding to the lower branch neutral stability point, where the instability wave decays exponentially, the principal contribution to ψ_0 is still provided by the particular solution (2.6a). In contrast, if the wall inhomogeneity is located far downstream of the lower branch, the contribution from the instability wave generated close to the leading edge may become comparable to that from ψ_{0p}. Since we are interested in the generation of the instability wave and not its scattering due to a wall inhomogeneity, we ignore any contribution to $\psi_0(x, Y)$ from eigensolutions generated upstream of the wall inhomogeneity.

Noting that the base flow quantities Ψ_0 and ψ_{0p} depend only upon the global coordinate x in the streamwise direction, we can expand them both as Taylor series in x about the origin to obtain

$$\Psi_0(x,Y) = \hat{\Psi}_0(Y) + \hat{\Psi}_{0x}(Y)\, x + O(x^2)\,, \tag{2.7a}$$

and

$$\psi_{0p}(x,Y) = \hat{\psi}_{0p}(Y) + \hat{\psi}_{0px}(Y)\, x + O(x^2)\,, \tag{2.7b}$$

where subscript x represents the partial derivative with respect to x and the superscript $\hat{}$ denotes the profile of a function at the origin. Since $x = O(\epsilon_l)$ within the local region, Eqs. (2.7a,b) imply that the streamwise variations of $\Psi_0(x,Y)$ and $\psi_0(x,Y)$ in the local region can be neglected to $O(\epsilon_l)$. Thus, both the steady and unsteady base flow solutions within the local region correspond to a parallel shear flow given by their respective profiles at the origin. This leads to a considerable simplification in the solution procedure for the steady and unsteady short-scale perturbations $\Psi_1^{(j)}$ and $\psi_1^{(j)}$, $j = 1-3$. The coefficient functions in the governing equations for these local perturbations are now independent of any streamwise coordinate, thus allowing these equations to be reduced to ordinary differential equations after taking a Fourier transform. The rest of this section essentially considers the solution for the short-scale perturbations $\Psi_1^{(j)}(X,Y)$ and $\psi_1^{(j)}(X,Y)$.

First consider the mean flow perturbations, $\Psi_1^{(1)}(X,Y)$ and $\Psi_1^{(3)}(X,Y)$, due to the local variations in wall suction velocity and wall height, respectively. Note that the wall admittance variation is manifested only through the unsteady boundary condition (2.2b). Therefore, to the leading order, there is no perturbation to the mean flow for the $j = 2$ case, and $\Psi_1^{(2)}(X,Y) \equiv 0$. Substituting the perturbation expansion (2.5) into (2.1)-(2.4), collecting terms of $O(\epsilon_w^{(j)})$, and transforming the resultant equation using the following definition for the Fourier transform,

$$\bar{g}(\alpha) = \frac{1}{\sqrt{2\pi}} \int_{-\infty}^{\infty} e^{-i\alpha X} g(X) dX \qquad , \tag{2.8}$$

one finds that $\bar{\Psi}_1^{(1)}(Y)$ and $\bar{\Psi}_1^{(3)}(Y)$ satisfy the time independent form of the Orr-Sommerfeld (O-S) equation in the wavenumber space

$$i\alpha\hat{\Psi}_0'(\frac{d^2}{dY^2} - \alpha^2)\bar{\Psi}_1 - i\alpha\hat{\Psi}_0'''\bar{\Psi}_1 - \frac{1}{R_{\delta^*}}(\frac{d^2}{dY^2} - \alpha^2)^2\,\bar{\Psi}_1 = 0\ , \tag{2.9}$$

subject to the inhomogeneous set of wall boundary conditions

$$\bar{\Psi}_1^{(1)}(0) = -\bar{F}^{(1)}(\alpha)/i\alpha\ , \quad \bar{\Psi}_1^{(1)\prime}(0) = 0\ , \tag{2.10a,b}$$

and

$$\bar{\Psi}_1^{(3)}(0) = 0\,, \quad \bar{\Psi}_1^{(3)\prime}(0) = -\hat{\Psi}_0''(0)\, F^{(3)}(\alpha)\,, \qquad (2.11a,b)$$

where the primes denote derivatives with respect to Y and the boundary condition for $\bar{\Psi}_1^{(3)}$ has been shifted to $Y = 0$ using a Taylor expansion in Y. Both $\bar{\Psi}_1^{(1)}$ and $\bar{\Psi}_1^{(3)}$ satisfy homogeneous boundary conditions far away from the wall,

$$\bar{\Psi}_1^{(j)} = \bar{\Psi}_1^{(3)\prime} = 0,\ j = 1,3,\ \text{as}\ Y \to \infty. \qquad (2.12a,b)$$

Although the term involving $d^4\Psi_1^{(j)}/dY^4$ in (2.9) is nominally $O(R_{\delta^*}^{-1})$, it has been retained in order to satisfy the no-slip boundary condition at the wall. This reflects the singular nature of the problem. Equation (2.9) contains additional terms which are uniformly $O(R_{\delta^*}^{-1})$ and, therefore, cannot be justified on a rational basis. A strictly rational perturbation scheme for the short-scale perturbations $\Psi_1^{(j)}, j = 1,3$ corresponds to the well-known triple deck theory. However, it involves different expansions in three separate regions in the direction normal to the wall (Stewartson[14]). In contrast, Eq. (2.9) describes the motion in the entire local region and also accounts for the finite Reynolds number effects more accurately than just a single term triple deck expansion.

The time independent Orr-Sommerfeld equation along with boundary conditions (2.11a,b) and (2.12a,b) also describes the perturbation to a parallel shear flow over an infinite flat plate due to small amplitude, sinusoidal variations in wall height. Approximate, analytical solutions to this problem were first obtained by Benjamin[15]. He also treated the case of a flow over an isolated bump as a superposition of the wavy wall solutions. Subsequently, Lessen and Gangwani[16] and Aldoss and Reshotko[17] integrated the Orr-Sommerfeld equation numerically to calculate the stationary wavy-wall solutions. We also find the solutions for $\bar{\Psi}_1^{(1)}$ and $\bar{\Psi}_1^{(3)}$ numerically by using a spectral collocation scheme on a staggered grid which has been described in detail by Macaraeg *et al*[18]. Note that the total mean flow perturbation can be obtained by computing the solution for all Fourier wavenumbers and then inverting the Fourier transform. However, the focus of this work is to determine the amplitude of the generated instability wave. It will be seen that with this limited objective, it is sufficient to solve (2.9)-(2.12) for a single Fourier mode corresponding to the (complex) wavenumber of the instability wave in the local region.

Having obtained the short-scale mean flow perturbation, we now analyze the short-scale correction, $\psi_1^{(j)}$, to the unsteady base flow solution. Substituting the perturbation expansion (2.5) into (2.1), collecting terms of $O(\epsilon_w^{(j)}\epsilon_{fs})$, and introducing the Fourier transform (2.8) leads to the O-S equation with a source term which is nonzero for $j = 1$ and $j = 3$

$$-i\omega(\frac{d^2}{dY^2} - \alpha^2)\bar{\psi}_1^{(j)} + i\alpha\hat{\Psi}_0'(\frac{d^2}{dY^2} - \alpha^2)\bar{\psi}_1^{(j)} - i\alpha\hat{\Psi}_0'''\bar{\psi}_1^{(j)}$$

$$-\frac{1}{R_{\delta^*}}\left(\frac{d^2}{dY^2}-\alpha^2\right)^2\bar{\psi}_1^{(j)} = -i\alpha\{\hat{\psi}'_{0p}\left(\frac{d^2}{dY^2}-\alpha^2\right)\bar{\Psi}_1^{(j)} - \hat{\psi}'''_{0p}\bar{\Psi}_1^{(j)}\} \ , \qquad (2.13)$$

As seen from (2.13), the forcing term on the right hand side arises due to the interaction of the short-scale mean flow perturbation with the unsteady base flow term ψ_0. Since the wall admittance variation does not cause any mean flow perturbation, the source term is identically zero for the $j = 2$ case.

Utilizing the perturbation expansion (2.5) along with (2.2)-(2.3), one finds that $\bar{\psi}_1^{(1)}$ satisfies the homogeneous boundary conditions at the wall

$$\bar{\psi}_1^{(1)}(0) = \bar{\psi}_1^{(1)\prime}(0) = 0 \ . \qquad (2.14a,b)$$

Although $\bar{\psi}_1^{(2)}$ satisfies a homogeneous governing equation, it has to satisfy the inhomogeneous boundary condition corresponding to the unsteady mass-flux through the porous surface

$$\bar{\psi}_1^{(2)}(0) = \bar{F}^{(2)}(\alpha)/i\alpha \ , \qquad (2.15a)$$

in addition to the no-slip boundary condition

$$\bar{\psi}_1^{(2)\prime}(0) = 0 \ . \qquad (2.15b)$$

On the other hand, shifting the boundary conditions for $\bar{\psi}_1^{(3)}$ to $Y = 0$ leads to

$$\bar{\psi}_1^{(3)}(0) = 0, \ \ \bar{\psi}_1^{(3)\prime}(0) = -\hat{\psi}''_0(0)\ \bar{F}^{(3)}(k) \ , \qquad (2.16a,b)$$

thus implying that $\bar{\psi}_1^{(3)}$ satisfies an inhomogeneous boundary condition as well as the inhomogeneous differential equation. The inhomogeneous boundary condition (2.16b) can be viewed as arising due to the adjustment of the base unsteady solution ψ_0 to the locally deformed wall geometry. Finally, the streamfunctions $\bar{\psi}_1^{(j)}$, $j = 1-3$ satisfy the homogeneous boundary conditions far away from the wall,

$$\bar{\psi}_1^{(j)} = \bar{\psi}_1^{(j)\prime} = 0 \ , j = 1-3, \ \text{ as } \ Y \to \infty \qquad (2.17a,b)$$

Thus, as pointed out by Reshotko[19], the receptivity problem in each case reduces to an inhomogeneous boundary value problem where the inhomogeneity is characteristic of the particular receptivity mechanism. Criminale[20] and Tam[21] also developed receptivity theories based on the O-S equation subject to forcing; however, this forcing amounted simply to an inhomogeneous boundary condition corresponding to the free-stream disturbance under consideration and did not involve any short-scale structure, a necessary ingredient for receptivity as discussed in the introduction. On the other hand, the present finite Reynolds number approach is similar in spirit to the large Reynolds number asymptotic approach of Goldstein[2]

and Ruban[3]. One may, in fact, view the present approach as recasting Goldstein and Ruban's triple-deck formulation in terms of the more familiar Orr-Sommerfeld framework.

The solution for $\psi_1^{(j)}$ in the physical space is given by the inverse Fourier integral

$$\psi_1^{(j)}(X,Y) = \frac{1}{\sqrt{2\pi}} \int_{-\infty}^{\infty} e^{i\alpha X} \bar{\psi}_1^{(j)}(\alpha, Y) d\alpha \quad . \tag{2.18}$$

where the integration path in the complex k plane is chosen to satisfy the causality requirements, i.e., such that the time harmonic solution under consideration here corresponds to the time-asymptotic limit of the corresponding initial value problem. Since we are only interested in the generated instability wave which propagates downstream (i.e., $X > 0$), the integration contour can be closed in the upper half α plane. Applying the Cauchy's integral theorem shows that the inverse Fourier integral corresponds to a sum of contributions from the various singularities of the integrand in (2.18). These include the pole contributions from the discrete spectrum and branch cut contributions from the continuous spectrum of the Orr-Sommerfeld operator. The unsteady motion associated with the generated T-S wave is then given by the residue contribution corresponding to the pole at the T-S wavenumber α_{T-S}, the location of which is determined numerically by solving the O-S eigenvalue problem. The residue contribution is related to the Fourier transform solution $\bar{\psi}_1^{(j)}$ by

$$\psi_1^{(j)}{}_{T-S}(X,Y) = \frac{\sqrt{2\pi}\, i}{\frac{\partial \bar{\psi}_1^{(j)-1}}{\partial \alpha} | \alpha = \alpha_{T-S}} e^{i\alpha_{T-S} X} \, . \tag{2.19}$$

We evaluated the right hand side of (2.19) by solving the inhomogeneous O-S problem using the spectral collocation scheme of Macaraeg *et al*[18], and computing the derivative in the spectral space, $\frac{\partial \bar{\psi}_1^{(j)-1}}{\partial \alpha}$ via a central difference approximation.

In experiments, it is customary to measure $u_{T-S}^{(j)*}$, the streamwise velocity fluctuation associated with the T-S wave. Therefore, using (2.19) and noting that the inhomogeneous terms in (2.13)-(2.17) are linear in $\bar{F}^{(j)}(\alpha)$, one can express $u_{T-S}^{(j)*}$ in the following form

$$u_{T-S}^{(j)*}(X,Y,t) = C_u^{(j)}\, u_{ac}^*\, E_u(Y;\, \omega, R_{\delta^*})\, e^{i(\alpha_{T-S} X - \omega t)} \, , \tag{2.20a}$$

where

$$C_u^{(j)} = \epsilon_w^{(j)} \bar{F}^{(j)}(\alpha_{T-S}) \Lambda_u^{(j)}(\omega, R_{\delta^*}) \, , \tag{2.20b}$$

and $E_q(Y;\, \omega, R_{\delta^*})$ denotes the instability wave eigenfunction for the physical quantity denoted by q. The eigenfunctions for different flow variables have been normalized in such a way that maximum of $E_u(Y;\, \omega, R_{\delta^*})$, the eigenfunction corresponding

to the streamwise velocity fluctuation, is equal to unity. The factor $\bar{F}^{(j)}(\alpha_{T-S})$ is the transform of the spatial distribution of the wall inhomogeneity, evaluated at the complex wavenumber $\alpha_{T-S}(\omega; R_{\delta^*})$ of the instability wave. In contrast, the function $\Lambda_u^{(j)}$ depends upon the external-disturbance frequency, ω, and location of the wall-inhomogeneity, R_{δ^*}, but is independent of the local geometry. We refer to it as the "efficiency function" for the particular combination of wall-inhomogeneity and free-stream disturbance.

The product $C_u^{(j)}$ relates the amplitude of the generated instability wave (at the location corresponding to the origin) to the amplitude of the incident free-stream disturbance. Hence, $C_u^{(j)}$ may be refered to as the "local coupling coefficient". Since we had remarked earlier about the similarity of the present method with the asymptotic approach, it should not come as a surprise that the expression (2.20b) for the coupling coefficient is identical in form to the asymptotic results of Goldstein[2] and Choudhari[5]. Equation (2.20b) echoes a generic result which is valid for all types of linear localized receptivity mechanisms. Essentially, it states that the effects of local geometry can be decoupled from the coupling coefficient in a very simple manner. This enables one to compare different types of localized mechanisms solely on the basis of their efficiency functions $\Lambda^{(j)}$, irrespective of the local geometry.

One should note that the values of the coupling coefficient $C^{(j)}$, and hence the efficiency function $\Lambda^{(j)}$, are inherently dependent upon the physical quantity chosen for measuring the instability wave amplitude. However, having found the streamwise velocity fluctuation produced by the generated T-S wave, the residue contributions for other flow variables can be determined easily by using the T-S eigenfunction for this quantity. For instance, if one measures the pressure fluctuation at the wall, $p_{T-S}^{(j)*}(Y = 0)$, instead of the maximum streamwise velocity fluctuation, one can write,

$$p_{T-S}^{(j)*}(X, Y = 0, t) = C_p^{(j)}\, \rho^* u_{ac}^* U_\infty^*\, e^{(\alpha_{T-S} X - \omega t)}\,, \tag{2.21a}$$

where

$$C_p^{(j)} = \epsilon_w^{(j)}\ \ \bar{F}^{(j)}(\alpha_{T-S})\ \ \Lambda_p^{(j)}(\omega, R_{\delta^*})\,, \tag{2.21b}$$

where the efficiency function $\Lambda_p^{(j)}$ is related to $\Lambda_u^{(j)}$ by

$$\Lambda_p^{(j)} = E_p(Y = 0;\ \omega, R_{\delta^*})\ \ \Lambda_u^{(j)} \tag{2.21c}$$

In the following section we present results illustrating the variation of the efficiency functions $\Lambda_u^{(j)}(\omega, R_{\delta^*})$ and $\Lambda_p^{(j)}(\omega, R_{\delta^*})$ with the frequency parameter and location of the wall inhomogeneity. In computing these results, we have used an approximation for the base unsteady solution ψ_{0p} obtained by using just the leading order term in (2.6b). Computations were also performed using all three terms from (2.6b),

and yielded visually indistinguishable results in all cases used for comparison. The reasons for truncating the expansion for ψ_{0_p} and its implications on the theoretical accuracy of the present approach are discussed in Section 4.

3. RESULTS

First consider the variation in the efficiency functions with the frequency of the external disturbance for a fixed location of the wall inhomogeneity. As pointed out in the previous section, the efficiency function has a different value depending on the physical quantity used to measure the amplitude of the generated instability wave. To begin with, let us analyze the behaviour of $\Lambda_u^{(j)}$, the complex valued efficiency functions based upon the maximum streamwise velocity fluctuation. In Figs. (3a-3c) and (4a-4c) we have plotted the magnitudes and arguments, respectively of $\Lambda_u^{(j)}, j = 1 - 3$, as functions of the frequency parameter $f = \omega^* \nu^* / {U_\infty^*}^2$, with the local Reynolds number $R \equiv \sqrt{Re_{\ell^*}}$ as a parameter. For the self-similar Blasius boundary layer, R is related to R_{δ^*}, the Reynolds number based on the local displacement thickness, via the simple relation $R = R_{\delta^*}/1.72$. Note that the local parameters ω and R_{δ^*} were used in Section 2 to formulate the problem since the analysis presented herein is valid even for non-similar boundary layer profiles. However, for the specific case of a Blasius boundary layer, it is more convenient to present the results in terms of the parameters f and R. The symbols in Figs. (3a-3c) correspond to results obtained using the present (O-S) approach, while the lines represent single term asymptotic predictions based on Goldstein[2] and Choudhari[5]. Except in obvious cases or when stated explicitly, the same notation will be followed in the remaining figures in this section which involve both symbols and lines. The first part of this Section focuses only on the results obtained using the O-S approach, while the latter part presents a detailed discussion regarding the comparison of these two approaches.

Three different locations of the wall inhomogeneity have been considered in Figs. (3a-3c). The location nearest to the leading edge corresponds to $R = 350$, and probably represents the lower bound on the range of Reynolds numbers in which the present approach can be expected to be valid. The next wall inhomogeneity location corresponds to $R = 700$, while the location farthest from the leading edge is assumed to be at $R = 1050$, i.e., in the range of Reynolds numbers where transition is expected to set in on a flat plate without suction. In presence of wall suction, the onset of transition may be delayed to much larger values of R. However, since the T-S waves leading to transition are usually generated much farther upstream of the transition location, receptivity locations corresponding to $R > 1050$ are not likely to be important in practice. For reference, the local growth rate of the generated T-S wave at each of these locations has been plotted in Fig. 5 as a function of the frequency parameter, f. In addition, the lower and upper branch frequencies at

the three stations have been marked on the horizontal axis in Figs. 3a-3c by the respective symbols, provided these frequencies fall in the range displayed in these figures.

From Figs. (3a-3c), one can observe two distinct trends in the behaviour of $|\Lambda_u^{(j)}(f)|$ depending on the type of wall inhomogeneity. For the wall suction (j=1) and wall admittance (j=2) cases, the value of f corresponding to the largest magnitude of the efficiency function is less than one fourth of the lower branch neutral frequency, $f_{l.b.}$, at both $R = 700$ and $R = 1050$. For larger frequencies, both $|\Lambda_u^{(1)}|$ and $|\Lambda_u^{(2)}|$ decrease monotonically until $f \approx f_{u.b.}$, the frequency parameter corresponding to the upper branch of the neutral stability curve. On the other hand, the magnitude of $\Lambda_u^{(3)}$, the efficiency function in the wall hump case (j=3), increases monotonically with f until reaching its maximum somewhere in the vicinity of $f = f_{u.b.}$ (see also Fig. 15b). The rate of increase in $|\Lambda_u^{(3)}|$ is fairly rapid in the range of subcritical frequencies ($f < f_{l.b.}$), but rather slow in the unstable range corresponding to $f_{l.b.} < f < f_{u.b.}$. One may also observe that the peak value of $|\Lambda_u^{(3)}|$ is nearly independent of the wall inhomogeneity location, being in the range 0.46-0.48 for all three locations of the roughness element. Subsequent to the point of its maximum, $|\Lambda_u^{(3)}(f)|$ was found to decrease rapidly, being smaller than 0.1 for most frequencies larger than $f_{u.b.}$. This behavior suggests that at any given location, the efficiency of receptivity due to a wall hump is highest for frequencies which are locally unstable. Finally, Figs. 4a-4c show that the arguments of the complex valued efficiency functions $\Lambda_u^{(3)}(f), j = 1 - 3$ change rather slowly in the frequency range of interest.

In Figs. 6a-6c, the magnitudes of $\Lambda_p^{(j)}$, the efficiency functions based upon the wall pressure fluctuation produced by the T-S wave are plotted as functions of f for the same locations of the wall inhomogeneity as in Figs. 3a-3c. One may observe from Fig. 6a that for small values of the frequency parameter, $|\Lambda_p^{(1)}|$ increases at a nearly constant rate, in a manner similar to that of $|\Lambda_u^{(1)}|$ in Fig. 3a. However, the value of $|\Lambda_p^{(1)}|$ continues to increase until f reaches approximately one-half of the lower branch neutral frequency, $f_{l.b.}$. On the other hand, the function $|\Lambda_u^{(1)}|$, which exhibits a boundary layer type behaviour in the range $f << f_{l.b.}$, has its maximum near $f < f_{l.b.}/4$. Furthermore, Fig. 6a shows that $|\Lambda_p^{(1)}|$ remains virtually constant following the initial region of constant slope. This behaviour is markedly different from that of $|\Lambda_u^{(1)}|$ which decreases monotonically in the range of larger frequencies.

The behaviour of $|\Lambda_p^{(2)}|$, the magnitude of the efficiency function in the wall admittance case, is quite similar to that of $|\Lambda_p^{(1)}|$ corresponding to the wall suction case discussed in the previous paragraph. The only qualitative difference between $|\Lambda_p^{(1)}|$ and $|\Lambda_p^{(2)}|$ is that the latter displays a slight overshoot near $f \approx f_{l.b.}/4$, and subsequently, a small dip in the unstable range $f_{l.b.} < f < f_{u.b.}$. Therefore, the previous

discusssion regarding the differences between $|\Lambda_p^{(1)}|$ and $|\Lambda_u^{(1)}|$ also holds in the case of $|\Lambda_p^{(2)}|$ and $|\Lambda_u^{(2)}|$. Finally, it is apparent from a comparison of Figs. 3c and 6c that the efficiency functions $\Lambda_u^{(j)}$ and $\Lambda_p^{(j)}$ possess different trends even in the case of receptivity due to a wall geometry variation (j=3). The function $|\Lambda_p^{(3)}(f)|$ does not exhibit the plateau behaviour displayed by $|\Lambda_u^{(3)}(f)|$ in the range of unstable frequencies, $f_{l.b.} < f < f_{u.b.}$. In fact, $|\Lambda_p^{(3)}(f)|$ has a nearly linear behaviour for all frequencies of interest (i.e., $f < f_{u.b.}$). Thus, one may conclude that irrespective of the type of wall inhomogeneity, the frequency response of a given receptivity mechanism is quite different depending on the specific flow quantity used to quantify the receptivity.

It was shown in Section 2 that the boundary value problem governing the short-scale unsteady perturbation involves a different kind of inhomogeneity depending on the particular agency inducing the short-scale variation. For instance, the receptivity due to a wall suction variation is entirely due to internal forcing representing the interaction of the Stokes wave with the short-scale mean flow perturbation. In contrast, the variation in the wall admittance leads to receptivity via only a forcing at the boundary corresponding to the short-scale unsteady mass flux through the porous surface. Finally, the boundary value problem for the receptivity due to a wall hump contains an inhomogeneous term in both the governing differential equation as well as in one of wall boundary conditions. As in the wall suction case, the source term in the differential equation arises due to an interaction of the Stokes wave with the mean flow perturbation, while the inhomogeneous boundary condition represents the direct scattering of the Stokes wave by the wall geometry variation. Figures 7a and 7b illustrate the nature of the source term in the differential equation governing the receptivity due to wall suction and wall geometry variations, respectively. In both figures, we have plotted the forcing function on the right hand side of Eq. (2.13) as a function of the transverse coordinate Y. The location of the receptivity region has been assumed to be fixed at $R = 1050$, and results have been plotted for five different values of the frequency parameter f. One may observe that for each frequency, the shape of the forcing function in Fig. 7a is quite different from that in Fig. 7b. The magnitude of the forcing function in the wall suction case is maximum at the wall and decreases rapidly away from it. On the other hand, the forcing function in the case of receptivity due to wall roughness has two lobes. The inner lobe is narrower, occupying less than one third of the boundary layer displacement thickness for most frequencies within the unstable range. The peak corresponding to the inner lobe also represents the maximum of the forcing function across the entire boundary layer. The maximum corresponding to the outer lobe is nearly one half of the maximum of the inner lobe. Figures 7a and 7b also show that in general, the magnitude of the forcing function is significant only within distances less than one half of the boundary layer displacement

thickness away from the wall. Thus, it seems reasonable to conclude that the energy transfer from the acoustic wave to the T-S wave is localized to the region close to the surface.

In order to assess the effectiveness of the two types of inhomogeneous terms leading to receptivity in the case of wall roughness, we have plotted their contributions separately in Fig. 8 along with the sum total. The dashed curve in Fig. 8 corresponds to contribution to the efficiency function $|\Lambda_u^{(3)}|$ due to the inhomogeneous term in the differential equation, while the dotted curve represents the contribution from the inhomogeneous boundary condition. The roughness element is assumed to have been fixed at a location corresponding to $R = 2800$ and the different contributions to the efficiency function have been plotted as functions of f. Figure 8 suggests that at all frequencies, the contribution due to the inhomogeneous boundary condition is much larger than that due to the interaction of the Stokes wave with the mean flow gradients. In fact, the latter contribution is nearly out of phase with the former at all values of the frequency parameter. Therefore, the magnitude of the efficiency function $|\Lambda_u^{(3)}|$ is approximately equal to the difference of the magnitudes of contributions from the two inhomogeneous terms. The asymptotic theory (Goldstein[2]) predicts that for $f >> f_{l.b.}$, the mean flow perturbation becomes very small and hence the total efficiency function can be well approximated by the contribution due to the inhomogeneous boundary condition alone. However, Fig. 8 shows this not to be the case.

Figures (9a-c) illustrate the variation in $|\Lambda_u^{(j)}|, j = 1 - 3$, for a fixed frequency disturbance as the location of the wall inhomogeneity, R, is varied. For completeness, the arguments of the complex valued $\Lambda_u^{(j)}$ functions are plotted as functions of R in Figs. 10a-10c. Results are plotted for four different frequency parameters in the range $f = 20\text{x}10^{-6}$ to $f = 35\text{x}10^{-6}$. This particular range was selected based upon the corresponding values for the total amplification ratio (the N factor) of a fixed frequency T-S wave between the two branches of the neutral stability curve. As seen from Fig. (6.4) in Mack[22], an amplification ratio of e^9 is attained first by a T-S wave with frequency corresponding approximately to $f = 27\text{x}10^{-6}$. The approximate N factors for the smallest and largest values of the frequency parameter in the range shown in Figs. 9a-9c are equal to 7 and 11, respectively. Hence, according to the well-known e^N criterion (see Smith and Gamberoni[23], Van Ingen[24], as well as Bushnell and Malik[25]) the frequencies in this range are likely to be most important from the point of view of transition. For reference, the two neutral locations for each frequency parameter are indicated by arrows on the horizontal axes in Figs. 9a-9c. The growth rate variation with respect to the Reynolds number is shown in Fig. 11.

Figure 9a shows that the efficiency of receptivity due to wall suction variation is highest in the range of locations which are significantly upstream of the lower branch

of the neutral stability curve. The maximum value of $|\Lambda_u^{(1)}|$ occurs when the region of wall suction variation is located approximately two-thirds of the distance from the leading edge to the neutral location. At farther downstream locations, $|\Lambda_u^{(1)}|$ decreases, but only to reach a plateau close to the location where the streamwise growth rate of the T-S wave is at its maximum. The value of $|\Lambda_u^{(1)}|$ remains roughly constant between the locations corresponding to the maximum growth rate and the upper branch of the neutral stability curve. Shortly after the wave begins to decay again, $|\Lambda_u^{(1)}|$ drops rapidly to very small values. As remarked before, the behaviour of the $|\Lambda_u^{(1)}|$ curve beyond the location corresponding to the upper branch is of little practical interest. Figure 9b shows that similar to the wall suction case, the local efficiency of receptivity due to a wall admittance variation is highest when the variation occurs close to the leading edge. Of course, one must realize that the higher levels of efficiency close to the leading edge are offset by the larger magnitudes of the decay factors corresponding to the exponential decrease in the T-S wave amplitude upstream of the lower branch neutral location. One may further observe that $|\Lambda_u^{(2)}|$ decreases rapidly as the region of wall admittance variation moves away from the leading edge. However, the rapid decrease is halted when the wall inhomogeneity moves to locations within the unstable region. In fact, the value of $|\Lambda_u^{(2)}|$ increases slightly for locations close to the upper branch.

The behaviour of $|\Lambda_u^{(3)}|$ shown in Fig. 9c as a function of the wall inhomogeneoity location is quite similar to that in Fig 3c, where $|\Lambda_u^{(3)}|$ was plotted as a function of the frequency parameter with the wall inhomogeneity fixed at a particular location. Thus, $|\Lambda_u^{(3)}|$ increases rapidly until reaching the lower branch neutral location, but the increase is quite slow within the range of unstable locations. After crossing the upper branch location, $|\Lambda_u^{(3)}|$ again decreases rapidly to very small values. Note that the crude resemblance between the two sets of figures, 3a-3c and 9a-9c, could have been anticipated based on the qualitative equivalence between increasing downstream distance for a fixed physical frequency and increasing physical frequency at a fixed location. In fact, in the infinite Reynolds number limit, this equivalence can be quantified in terms of a similarity parameter $R^{3/2}F$ in the vicinity of branch I of the neutral stability curve.

The present analysis was based on the assumption that the local instability wavelength is much shorter than the length scale over which the mean boundary layer properties change significantly, i.e., the distance of the wall inhomogeneity from the leading edge. This assumption enables one to neglect the variation of the base flow over the length of the receptivity region. The validity of this approximation can be verified *a posteriori* from the results in Figs. 9a-9c. Essentially, the "local" approximation is valid if the efficiency function does not vary significantly over an instability wavelength. Figures 9a-9c show that the only region within the entire domain of interest where the efficiency functions, $|\Lambda_u^{(j)}|$, $j = 1 - 3$, have a large gra-

dient corresponds to locations close to the leading edge. For instance, at a location corresponding to $R = 500$, the variation in $|\Lambda_u^{(2)}|$ over an instability wavelength is O(10%) for $f = 30e-6$. Consequently, the receptivity predictions in the vicinity of this point can be assumed to be accurate only within a comparable bound for error.

In the remaining part of this paper, we compare the results obtained using the present approach with predictions based on the asymptotic (triple deck) framework used by previous investigators. As remarked before, the coupling coefficient in both cases can be expressed as a product of the geometry and efficiency functions, $\bar{F}^{(j)}$ and $\Lambda_u^{(j)}$, respectively. This allows us to compare the results of the two approaches by comparing separately their respective predictions of $\bar{F}^{(j)}$ and $\Lambda_u^{(j)}$. For a specified spatial destribution of the wall inhomogeneity, the geometry factor $\bar{F}^{(j)}(\alpha_{T.S.})$ depends only upon the instability wavenumber $\alpha_{T.S.}$ which is determined by an eigenvalue calculation. We already presented results for the imaginary part of $\alpha_{T.S.}$ in Fig. 5. This quantity is usually much smaller than the real part of $\alpha_{T.S.}$. However, it may have a significant impact on the value of $\bar{F}^{(j)}$ for certain types of geometries. Figure 5 shows that even though the triple deck expansions are valid only in the vicinity of the lower branch of the neutral stability curve, the asymptotic predictions for the streamwise growth rate, $Imag(\alpha_{T.S.})$, exhibit correct trends in most parts of the unstable region. Of course, since only a leading order solution was used to compute the asymptotic results, there are significant quantitative errors in comparison to the O-S results. For example, the asymptotic estimates for the maximum growth rate are consistently larger than the values predicted using the O-S equation. In Fig. 12 we show a comparison of the real parts of the instability wavenumber α_{T-S} calculated from the two methods. In contrast to the predictions for the imaginary part of α_{T-S}, one finds that the asymptotic theory always underestimates the value of $Real(\alpha_{T-S})$. The differences in $Real(\alpha_{T-S})$ may not be crucial for smooth geometries such that the geometry function $\bar{F}^{(j)}(\alpha)$ varies slowly enough with α. However, for shapes such as a rectangular hump, where $\bar{F}^{(j)}(\alpha)$ oscillates on the scale of the hump length, the asymptotic predictions may have a significant error. The errors in the asymptotic predictions for both $Real(\alpha_{T-S})$ and $Imag(\alpha_{T-S})$ become smaller for larger values of the Reynolds number, especially in the vicinity of $f_{l.b.}$ (Figs. 13a,13b). However, the extent of this improvement is quite marginal even for R as large as 2800.

Choudhari[5] utilized the triple deck theory to examine the influence of the width of a suction strip on the receptivity due to the interaction of a free-stream acoustic wave with the mean flow disturbance induced by a uniform suction applied through the strip. As discussed above, the local geometry enters only through the factor $\bar{F}^{(1)}$ which is simply the Fourier coefficient of the wall suction distribution corresponding to the T-S wavenumber, α_{T-S}, at the specified acoustic frequency, ω. Choudhari[5]

presented a graph illustrating the variation in $\bar{F}^{(1)}$ with respect to the width of the suction strip for four different locations of the strip. The geometry function $\bar{F}^{(1)}$ was evaluated using the asymptotic value of α_{T-S}. However, since the results were plotted with the suction-strip width normalized by the local T-S wavelength (i.e., as $2\pi w_{strip}/Real(\alpha_{T-S})$), the same plot can also be utilized in the context of the present finite Reynolds number approach by using the value of $Real(\alpha_{T-S})$ obtained from the O-S eigenvalue problem. The inferences drawn in this manner will be exact for the case of a wall inhomogeneity located at one of the neutral stations, but only qualitatively true for other locations for which $Imag(\alpha_{T-S})$ is nonzero.

In addition to the instability wavenumber α_{T-S}, it is useful to compare the finite Reynolds number and asymptotic predictions for $E_p(Y = 0)$ which also depends only upon the solution to the eigenvalue problem. This quantity represents the ratio of the wall pressure fluctuation and the maximum streamwise velocity fluctuation associated with the T-S wave, and relates the the two efficiency functions $\Lambda_p^{(j)}$ and $\Lambda_u^{(j)}$ as shown in (2.23c). Note that in the asymptotic theory, one has to deal with separate expansions in three different regions in the transverse direction, and the maximum of the streamwise velocity fluctuation can only be determined by forming a composite expansion which is uniformly valid in all three regions. For convenience, the predictions in Goldstein[2] and Choudhari[5] utilized an approximate value for this quantity based upon the maximum across the main part of the boundary layer, i.e., across the middle deck of the asymptotic expansion. The same approximation has also been used in the asymptotic results used in this paper. The fact that the maximum of the streamwise velocity eigenfunction across the lower deck is slightly larger than this approximate value, especially for frequencies much larger than the lower branch neutral frequency would indicate that the magnitude of $E_p(Y = 0)$ based on a composite asymptotic expansion will be somewhat smaller than the approximate result displayed here. In Fig. 14 we have plotted $|E_p(Y = 0)|$ as a function of f, with the wall inhomogeneity location as a parameter. One may observe that the agreement between the asymptotic and O-S results is quite satisfactory for $f < f_{l.b.}$. However, for frequencies corresponding to $f > f_{l.b.}$, the asymptotic predictions for $E_p(Y = 0)$ are somewhat smaller than the values obtained from the O-S equation. Recomputing the asymptotic result using the maximum streamwise velocity fluctuation across the lower deck led to reduced differences with the O-S predictions in the range $f > f_{l.b.}$. However, since the correct approach involves using the somewhat cumbersome composite expansion across all decks, all asymptotic predictions used in this paper are based on the maximum across the main deck.

We now return to the Figs. 3a-3c as well as Figs. 4a-4c, and compare the values of the efficiency fucntions $\Lambda_u^{(j)}$ obtained from the asymptotic and finite Reynolds

number approaches. Figure 3a shows that for the $j = 1$ case, i.e., for receptivity due to a wall suction variation, the agreement between the two approaches is quite good for frequencies close to $f_{l.b.}$, the frequency corresponding to the lower branch of the neutral stability curve. The agreement is not equally satisfactory in regions away from $f = f_{l.b.}$, but can still be considered reasonable. Figure 15a shows that a better overall comparison is possible at larger Reynolds numbers. On the other hand, it can be seen from Fig. 3b that in the case of receptivity due to a wall admittance variation, i.e., $j = 2$, the asymptotic predictions for $|\Lambda_u^{(j)}|$ are in excellent agreement with the finite Reynolds number results even at Reynolds numbers as low as 350. The only range of frequencies where the two predictions differ significantly corresponds to $f << f_{l.b.}$. Figure 3c shows that for $j = 3$, viz., receptivity due to a roughness element on the wall, the magnitudes of the $\Lambda_u^{(3)}$ function calculated using the two approaches match well at small frequencies, $f \leq f_{l.b.}$; however, as seen from Fig. 4c, the arguments of $\Lambda_u^{(3)}$ differ significantly. On the other hand, as f becomes larger than $f_{l.b.}$, the two predictions for the magnitude of $\Lambda_u^{(3)}$ begin to deviate from each other, but the agreement in the phase of $\Lambda_u^{(3)}$ improves substantially. The average difference in the magnitude predictions is of the order of 15-20 percent for $f_{l.b.} < f < f_{u.b.}$. Figure 15b shows that this difference persists at larger values of the Reynolds number. One may remark at this point that the asymptotic predictions of Goldstein[2] matched quite well with Aizin and Polykov's[26] experimental findings related to the receptivity due to the interaction of a free-stream acoustic wave with a hump on the wall. However, the overall asymptotic predictions were somewhat on the lower side of the range of T-S wave amplitudes measured in the experiments.

The above trends in the comparison of the asymptotic and finite Reynolds number approaches would suggest that predictions from the latter approach would match the experimental results even better. Finally, if one compares the efficiency functions based on the pressure fluctuation at the wall (Fig. 6c), an excellent agreement is found at all frequencies as well as Reynolds numbers. The differing comparison for the two types of efficiency functions, $\Lambda_u^{(j)}$ and $\Lambda_p^{(j)}$, can easily be explained on the basis of the comparison of $E_p(Y = 0)$ discussed previously in the context of Fig. 14.

The asymptotic theory has the advantage that it furnishes analytical solutions, thus enabling exhaustive parametric studies to be conducted without much cost. Therefore, in the absence of detailed numerical results, approximate results can be obtained by using the asymptotic predictions. The comparison between the two approaches in the preceding paragraphs showed that the triple deck theory predicts the overall trends correctly in most of the parameter space. However, there are significant quantitative errors in the asymptotic predictions related to the neutral curve as well as streamwise growth rates of the T-S waves. This may

affect the values of the geometry factor to a considerable extent. On the other hand, the asymptotic results related to the efficiency functions were found to be relatively more accurate. Therefore, as a first cut measure, the accuracy of the asymptotic predictions can be improved by calculating the geometry factor using an O-S result for the instability wavenumber. To investigate if the accuracy of the efficiency functions can be further improved by using a little additional information from a numerical data base obtained with a finite Reynolds number approach, the results from Fig. 3c for $R = 700$ and $R = 1050$ are replotted in Fig. 16 after normalizing both the ordinate, $|\Lambda_u^{(3)}|$, and the abscissa, f, by their respective values at the lower branch of the neutral stability curve. It is obvious that the significant discrepancies in Fig. 3c at larger frequencies have now disappeared, yielding an excellent agreement between the two approaches at all frequencies as well as wall inhomogeneity locations. This suggests a way of profitably utilizing any available asymptotic input without sacrificing the accuracy to any great extent. This type of correlation, if applicable, will be especially valuable for boundary layer flows more complex than the Blasius boundary layer, since the asymptotic theory may be less accurate in such cases.

4. APPLICATION TO RECEPTIVITY IN DISTRIBUTED REGIONS OF SHORT-SCALE VARIATIONS

The discussion in the previous sections was limited to receptivity occuring in localized regions of wall inhomogeneities. However, the results obtained therein can also be extended to receptivity occuring in distributed regions of short scale variations. The solution for the localized case can be utilized as part of a slowly varying Green's function for the problem of distributed receptivity in a manner similar to Tam[21] who used this idea earlier in a related context. According to the stability theory for weakly non-parallel shear flows, the uniformly valid solution for the streamwise velocity fluctuation sufficiently far downstream of a point source at $X = X_s$ is given by

$$G_u(X, Y; f \mid X_s) = A_0(x_s)A(x;\, x_s)E_u(Y,\, x;\, f)e^{i[\Theta(X)-\Theta(X_s)-\omega t]}, \qquad (4.1)$$

where the streamwise origin of the coordinate system has been fixed at some arbitrary point sufficiently far downstream of the leading edge. The initial amplitude, $A_0(x_s)$, in (4.1) is provided by the solution to the local problem at X=0 (i.e., the local coupling coefficient), with the geometry factor $\bar{F}^{(j)}(\alpha_{T.S.})$ set equal to unity corresponding to a point source excitation. The amplitude and phase functions, $A(x;\, x_s)$ and $\Theta(X)$ are obtained from the weakly non-parallel stability analysis.

Summing over the contributions from the entire source region, one would obtain,

$$u_{T-S} = \int_{-\infty}^{X} G_u(X, Y; f \mid X_s) F(X_s) dX_s, \tag{4.2}$$

where the function $F(X_s)$ now denotes the streamwise distribution of the forcing function in the equations describing the $O(\epsilon_{fs}\epsilon_w^{(j)})$ perturbation. For instance, in the wall admittance problem, it corresponds to the specified distribution of the unsteady vertical velocity. Thus given the streamwise distribution of the forcing function, the integral in Eq. (4.2) can be evaluated to determine the instability amplitude at any given station.

By differentiating with respect to the streamwise variable, Eq. (4.2) can also be converted to a wave amplitude equation similar to that obtained by Tam[21],

$$\frac{\partial u_{T-S}}{\partial X} = i \frac{\partial \Theta}{\partial X} u_{T-S} + F G_u + O(\epsilon_l). \tag{4.3}$$

Equation (4.3) shows that when the receptivity occurs continuously over a large number of instability wavelengths, the local change in the amplitude of the T-S wave is due to transfer of energy from the mean flow (in other words, the exponential growth or decay of instability waves generated upstream of the present location) as well as due to local input from the external disturbances. As pointed out by Tam, the relative contributions from the two types of inputs depend upon the local amplitude of the instability wave. Large values of the instability wave amplitude would imply that the contribution due to the external input is much weaker compared to the local amplification rate due to transfer of energy from the mean flow via the Reynolds stress distribution. Therefore, for locations close to the upper branch of the neutral stability curve, the amplitude distribution curve asymptotes to that of a pure T-S wave eigensoluion.

One may also remark in passing that for a spatially periodic forcing such as that induced by wall-waviness, or suction strips with uniform spacing, the contributions from neighbouring locations to the integral in (4.2) would tend to cancel each other. Therefore, the Green's function integral will be dominated by contributions from a small range of locations in the vicinity of the point where the integrand is nearly stationary. At this location, the instability phase Θ is maximally synchronized (or "tuned") with the phase of the external forcing F thus leading to a minimal cancellation in the surrounding region. In other words, the instability wave and the forcing function are closest to being in resonance in this region.

5. CONCLUDING REMARKS

An alternative to the triple deck approach was presented for the prediction of receptivity due to the interaction of a free-stream acoustic wave with localized regions of short-scale variations in surface boundary conditions. The receptivity problem reduces to an inhomogeneous Orr-Sommerfeld problem in the Fourier transform space, and the amplitude of the generated instability wave can be determined as the residue corresponding to the T-S wavenumber. This approach is non-asymptotic, but it has the advantage of being relatively more accurate at lower Reynolds numbers. The leading order error term is estimated to be $O(R_{\delta^*}^{-3/4}\ log\ R_{\delta^*})$ or $O(R_{\delta^*}^{-3/5}\ log\ R_{\delta^*})$ depending on whether the acoustic frequency scales on the frequency corresponding to the lower or upper branch of the neutral stability curve. Thus, at finite Reynolds numbers, the accuracy of this approach is limited only due to the "localness" approximation and freezing the profile of the undisturbed mean flow over this local region.

The above estimate for the error has been obtained on the assumption that one has used the full three term asymptotic expansion in (2.6b) to obtain the unsteady base flow solution, ψ_{0p}. Replacing ψ_{0p} by its leading order behaviour corresponding to the Stokes shear wave increases the theoretical estimate for the error to $O(x_1^{-1})$. For sufficiently large Reynolds numbers, this error is of $O(R_{\delta^*}^{-1/4})$ for f close to $f_{l.b.}$, which is comparable to the error in the single term triple deck expansion. However, the error in the finite Reynolds number approach becomes much smaller in the main part of the unstable region, since x_1^{-1} is of $O(R_{\delta^*}^{-2/5})$ there. Moreover, we compared the efficiency functions based on the Stokes wave approximation for ψ_{0p} with those obtained using the complete three term asymptotic expansion in (2.6a,b) for the case of a wall inhomogeneity located at $R = 1050$, and the two results were found to be visually indistinguishable on the scale of Figs. 3a,c.

Since the T-S wave amplitude is determined numerically, using three terms from (2.6b) is no more difficult than just the Stokes wave solution. However, a solution such as (2.6b) may not always be available, especially in more realistic flows corresponding to non-similar base mean flows. In fact, the only available information about the acoustic disturbance may consist of the local fluctuation in the free-stream velocity. Since the region of receptivity has been assumed to be a large number of convective wavelengths downstream of the leading edge, it seems reasonable to compute ψ_{0p} by assuming the airfoil surface to be locally flat and infinite in both directions. Then ψ_{0p} satisfies the O-S equation subject to the specified slip velocity in the free-stream. For incompressible flows the Stokes shear wave corresponds to the zero wavenumber (i.e., acoustic) solution to the O-S equation.To maintain a consistent way of approximating ψ_{0p} in all types of boundary layers, we have used the Stokes wave approximation even in the case of the self-similar Blasius boundary layer.

In addition to predicting the generation of the viscous T-S waves, the finite Reynolds number approach can be utilized to predict the coupling coefficients for the case of predominantly inviscid type instabilities in an adverse pressure gradient boundary layer where the triple deck framework is not applicable. In fact, with minor modifications, the present approach can be extended to such complex flows as three-dimensional and high-speed boundary layers. These flows are susceptible to various types of instability waves, each with its own asymptotic structure. In order to compare the effectiveness of a wall inhomogeneity in exciting the different types of instability waves, it becomes necessary to have a general approach which will be valid for as many of these instabilities as possible. It is for this class of problems that the strength of the approach presented in this paper really becomes apparent. Some preliminary results on the receptivity in high-speed and three-dimensional boundary layers using this approach have been presented by the present authors in Ref. [10]. Finally, the comparison of the present results with the asymptotic predictions suggests that in unsteady problems governed by the triple deck framework, quite satisfactory results can be obtained by using only a single term in the asymptotic expansion. In addition, such a comparison can also suggest ways of utilizing the asymptotic results with better accuracy, especially in more complicated problems such as those outlined above.

Acknowledgements

The authors would like to thank Dr. Michele Macaraeg for kindly providing the SPECLS code which served as a starting point for the finite Reynolds number receptivity calculations described in this paper. The first author is grateful to Dr. Mujeeb Malik for his continuous support as well as a number of stimulating discussions. Thanks are also due to Dr. Lian Ng for reviewing this manuscript. The research of the first author was supported by the Theoretical Flow Physics Branch, Fluid Mechanics Division, NASA Langley Research Center, Hampton ,VA under contract NAS1-18240.

References

1. Goldstein, M.E., "The evolution of Tollmien-Schlichting waves near a leading edge," *J. Fluid Mech.*, Vol. 127, pp. 59-81, 1983.

2. Goldstein, M.E., "Scattering of acoustic waves into Tollmien-Schlichting waves by small streamwise variations in surface geometry," *J. Fluid Mech.*, Vol. 154, pp. 509-529, 1985.

3. Ruban, A.I., "On the genaration of Tollmien-Schlichting waves by sound," Transl. in *Fluid Dyn.*, Vol. 19, pp. 709-16, 1985.

4. Goldstein, M.E., Leib, S. and Cowley, S., "Generation of Tollmien-Schlichting waves on interactive marginally separated flows," *J. Fluid Mech.*, Vol. 181, pp. 485-518, 1987.

5. Choudhari, Meelan, "Boundary Layer Receptivity Mechanisms Relevant to Laminar Flow Control", Ph.D. dissertation, University of Arizona, 1990.

6. Bodonyi, R.J., Welch, W.J.C., Duck, P.W. and Tadjfar, M , "A numerical study of the interaction between unsteady free-stream disturbances and localized variations in surface geometry," *J. Fluid Mech.*, Vol. 209, pp. 285-308, 1989.

7. Choudhari, Meelan and Kerschen, E.J., "Instability Wave Patterns Generated by Interaction of Sound Waves with Three-Dimensional Wall Suction or Roughness," AIAA Paper 90-0119, 1990.

8. Kerschen, E.J., "Boundary Layer Receptivity," AIAA Paper 89-1109, 1989.

9. Choudhari, Meelan and Kerschen, E.J., "Boundary Layer Receptivity due to Three-Dimensional Convected Gusts," Proceedings of ICASE/NASA LaRC Instability and Transition Workshop, Springer Verlag, 1990.

10. Choudhari, Meelan, and Streett, C.L., "Boundary Layer Receptivity Phenomena in Three-Dimensional and High-Speed Boundary Layers," AIAA Paper 90-5258, 1990.

11. Lighthill, M.J., "The Response of Laminar Skin Friction and Heat Transfer to Fluctuations in the Stream Velocity," *Proc. Roy. Soc., London*, Series A, Vol. 224, pp. 1-23, 1954.

12. Ackerberg and Phillips, "The Unsteady Laminar Boundary Layer on a Semi-infinite Flat Plate due to Small Fluctuations in the Magnitude of the Free-Stream Velocity," *J. Fluid Mech.*, Vol. 51, pp. 137-157, 1972.

13. Lam and Rott, N., "Theory of Linearized Time-Dependent Boundary Layers," Cornell University GSAE Rep. AFOSR TN-60-1100, 1960.

14. Stewartson, K., "Multistructured boundary layers on flat plates and related bodies," *Adv. Appl. Mech.*, Vol. 14, pp. 145-239, 1974.

15. Benjamin, Brooke, "Shearing Flow over a Wavy Boundary," *J. Fluid Mech.*, Vol. 6, Part 2, pp. 161-204, 1959.

16. Lessen, M. and Gangwani, "Effect of Small Amplitude Wall Waviness upon the Stability of the Laminar Boundary Layer," *Phys. Fluids*, Vol. 19, No. 4, pp. 510-513, 1976.

17. Aldoss and Reshotko, E., "Disturbances in a Laminar Boundary layer due to Surface Waviness or Roughness," FTAS/TR-80-151, Dept. of Mech. Aero. Eng., Case Western Reserve Univ., Sept. 1980.

18. Macaraeg M. G., Streett, C.L. and Hussaini, M.Y., "A Spectral Collocation Solution to the Compressible Stability Eigenvalue Problem," NASA-TP 2858, Dec. 1988.

19. Reshotko, E., "Boundary layer stability and transition," *Ann. Rev. Fluid Mech.*, Vol. 8, pp. 311-349, 1976.

20. Criminale, W., "Interaction of the Laminar Boundary Layer with Free-Stream Turbulence," *Phys. Fluids, Special Supplement*, pp. 101-107, 1967.

21. Tam, C.K.W., "The Excitation of Tollmien-Schlichting Waves in Low Subsonic Boundary Layers by Free-Stream Sound Waves," *J. Fluid Mech.*, Vol. 109, pp. 483-501, 1981.

22. Mack, L.M., "Boundary layer linear stability theory," AGARD Report 709, 1984.

23. Smith, A. M. O. and Gamberoni, N., "Transition, pressure gradient and stability theory," Douglas Aircraft Co., Rep. ES 26 388, El Segundo, Calif., 1956.

24. Van Ingen, J. L., "A suggested semi-empirical method for the calculation of the boundary-layer transition region," Univ. of Technology, Dept. of Aero. Eng., Rept. UTH-74, Delft, Holland, 1956.

25. Bushnell, D. M. and Malik, M. R., "Application of stability theory to laminar flow control - Progress and Requirements," Proc. Symp. on the Stability of Time Dependent and Spatially Varying Flows, NASA-Langley Research Center, Hampton, Virginia, Aug. 19-23, 1985, (eds. Dwoyer, D. L. and Hussaini, M. Y.), Springer, New York, pp. 1-17, 1987.

26. Aizin, L. B., Polyakov, M. F., "Acoustic Generation of Tollmien-Schlichting Waves over Local Unevenness of Surface Immersed in Stream (in Russian)," Preprint 17, Akad. Nauk USSR, Siberian Div., Inst. Theor. Appl. Mech., Novosibirsk, 1979.

(a) A region of short-scale variation in wall suction velocity.

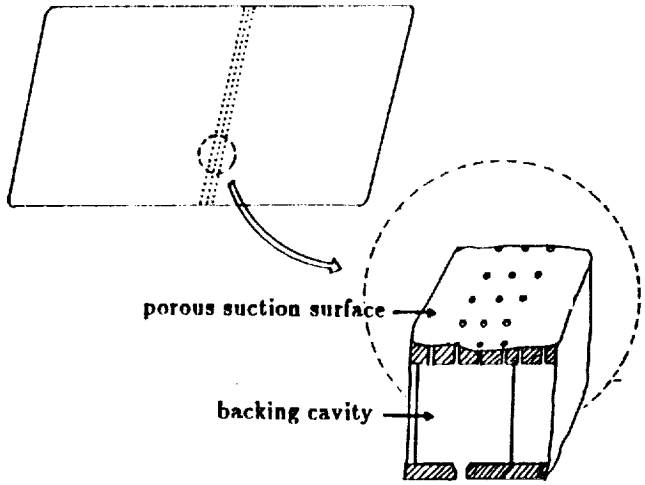

(b) A region of short-scale variation in wall admittance.

(c) A region of short-scale variation in wall geometry.

Fig. 1 Different types of wall inhomogeneities.

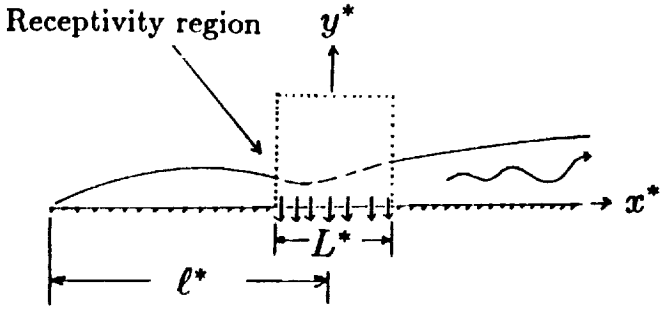

Fig. 2 Sketch of the coordinate system.

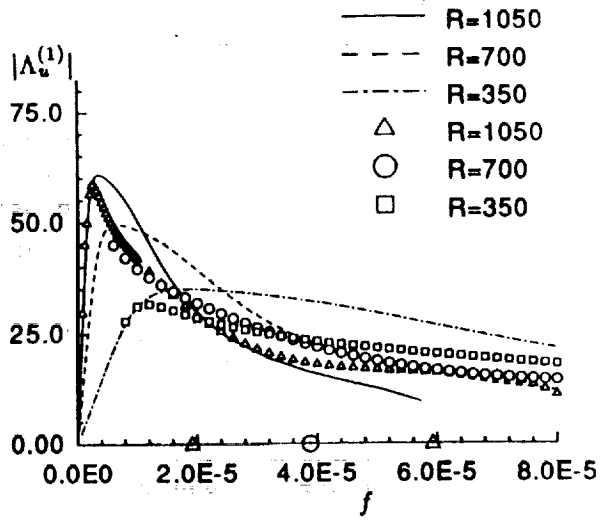

(a) Receptivity due to wall suction variation

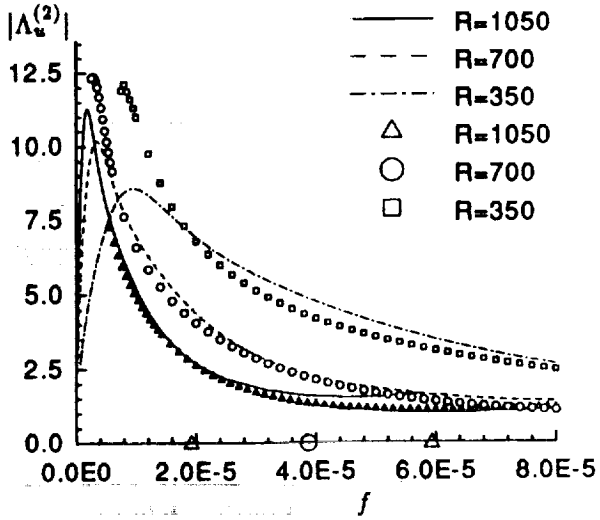

(b) Receptivity due to wall admittance variation

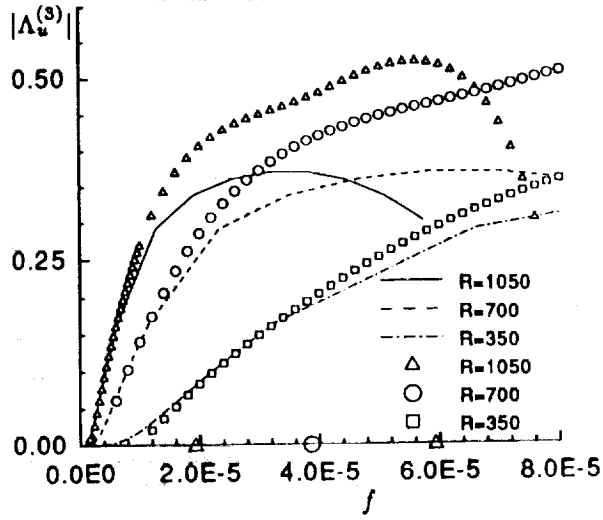

(c) Receptivity due to wall geometry variation

Fig. 3 Magnitudes of the efficiency functions $\Lambda_u^{(j)}, j = 1 - 3$ from Eq. (2.20b) as functions of the non-dimensional frequency parameter $f = \omega^* \nu_\infty^* / U_\infty^{*\,2}$, with the location of the wall inhomogeneity ($R \equiv \sqrt{Re_{\ell^*}} = R_{\delta^*}/1.72$) as a parameter. The symbols denote the results from the finite Reynolds number approach, while the lines correspond to asymptotic predictions.

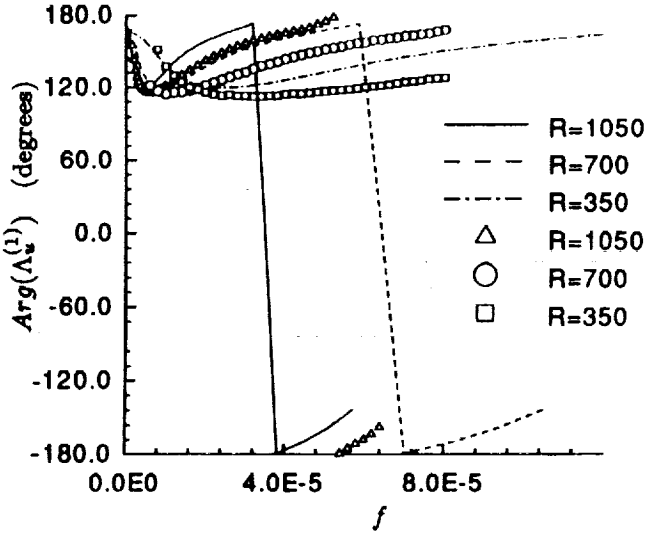

(a) Receptivity due to wall suction variation

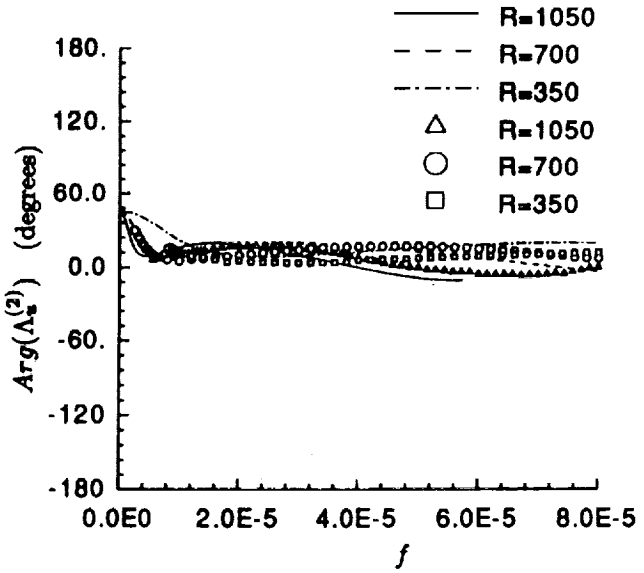

(b) Receptivity due to wall admittance variation

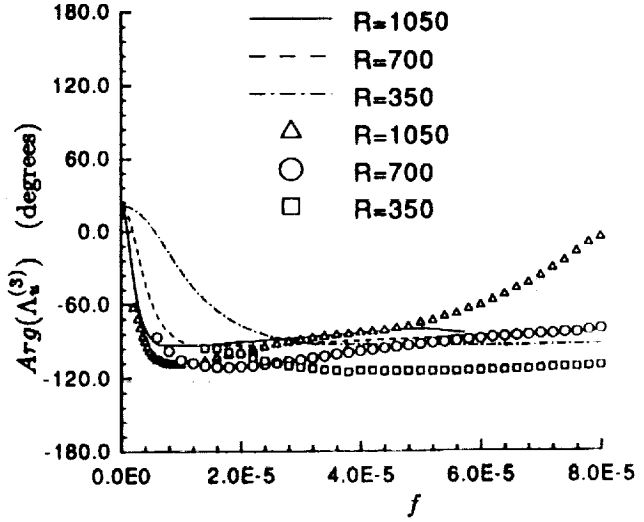

(c) Receptivity due to wall geometry variation

Fig. 4 Phase of the complex valued efficiency functions $\Lambda_w^{(j)}, j = 1 - 3$ from Eq. (2.20b) as functions of the non-dimensional frequency parameter $f = \omega^* \nu_\infty^* / U_\infty^{*2}$, with the location of the wall inhomogeneity ($R \equiv \sqrt{Re_{\ell^*}} = R_{\delta^*}/1.72$) as a parameter. The symbols denote the results from the finite Reynolds number approach, while the lines correspond to asymptotic predictions.

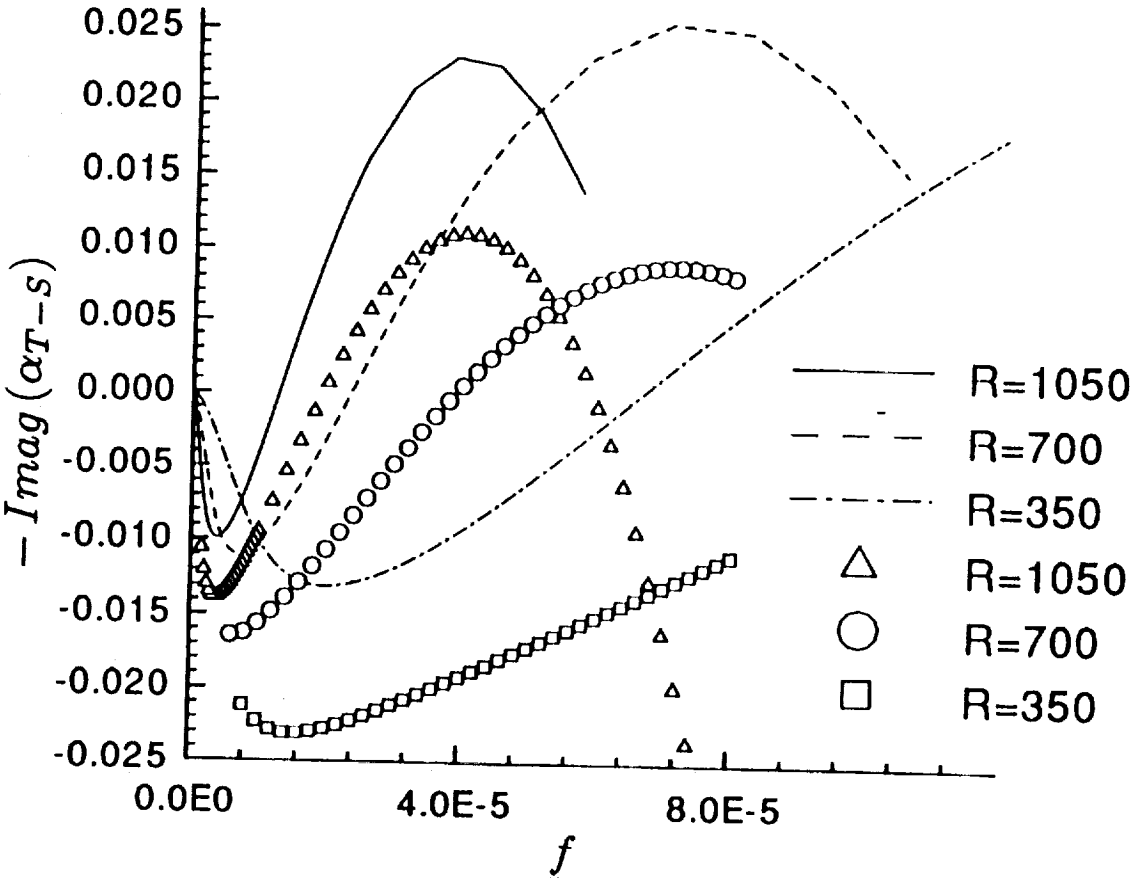

Fig 5 Streamwise growth rate, $-Imag(\alpha_{T-S})$, as a function of f for the same wall inhomogeneity locations as in Figs. 3 and 4.

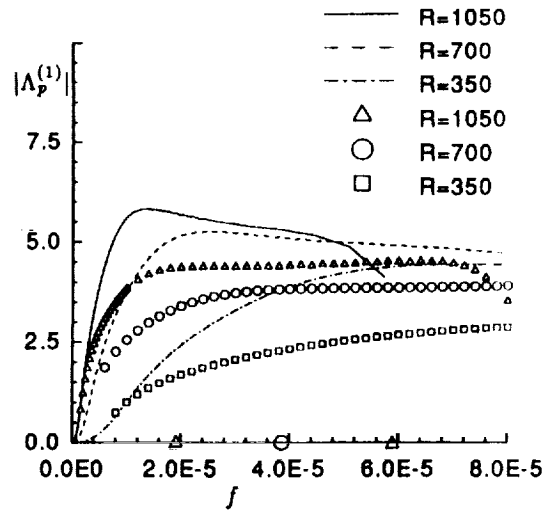

(a) Receptivity due to wall suction variation

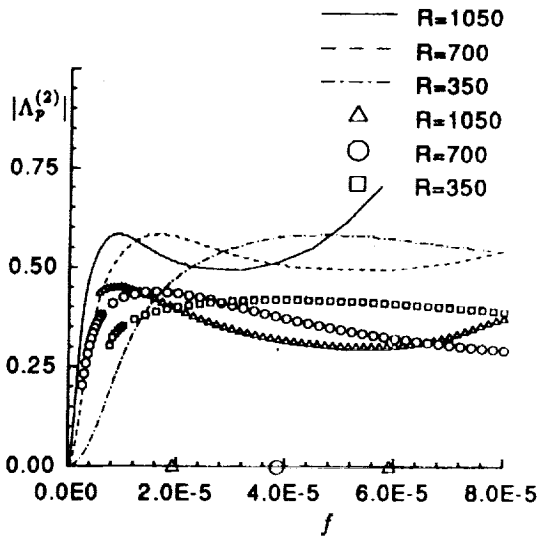

(b) Receptivity due to wall admittance variation

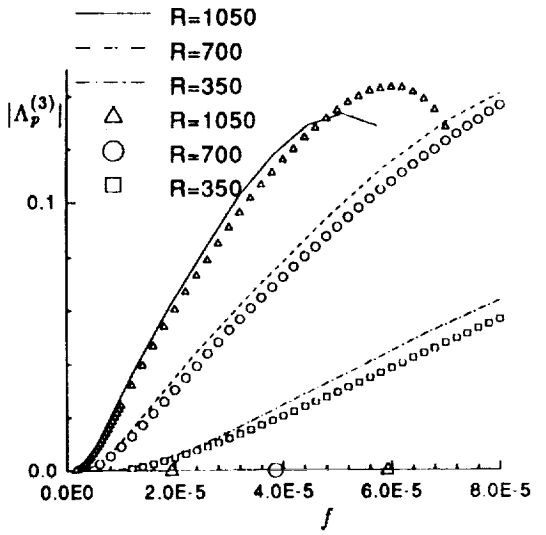

(c) Receptivity due to wall geometry variation

Fig. 6 Magnitudes of the efficiency functions $\Lambda_p^{(j)}, j = 1 - 3$ from Eq. (2.21b) as functions of the non-dimensional frequency parameter $f = \omega^* \nu_\infty^* / U_\infty^{*2}$, with the location of the wall inhomogeneity ($R \equiv \sqrt{Re_{\ell^*}} = R_{\delta^*}/1.72$) as a parameter. The symbols denote the results from the finite Reynolds number approach, while the lines correspond to asymptotic predictions.

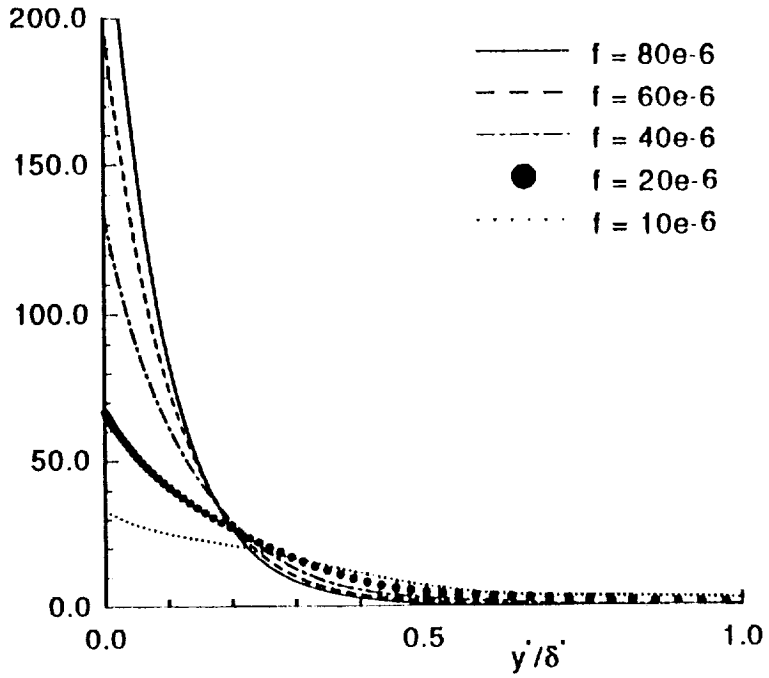

(a) Receptivity due to wall suction variation

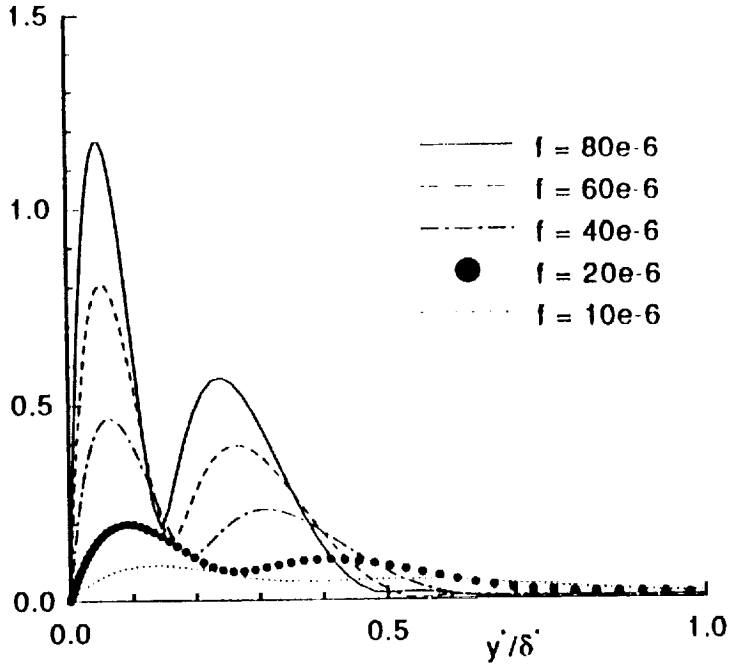

(b) Receptivity due to wall geometry variation

Fig. 7 The forcing function on the right hand side of (2.13) as a function of the transverse coordinate $Y = y^*/\delta^*$ ($R = 1050$).

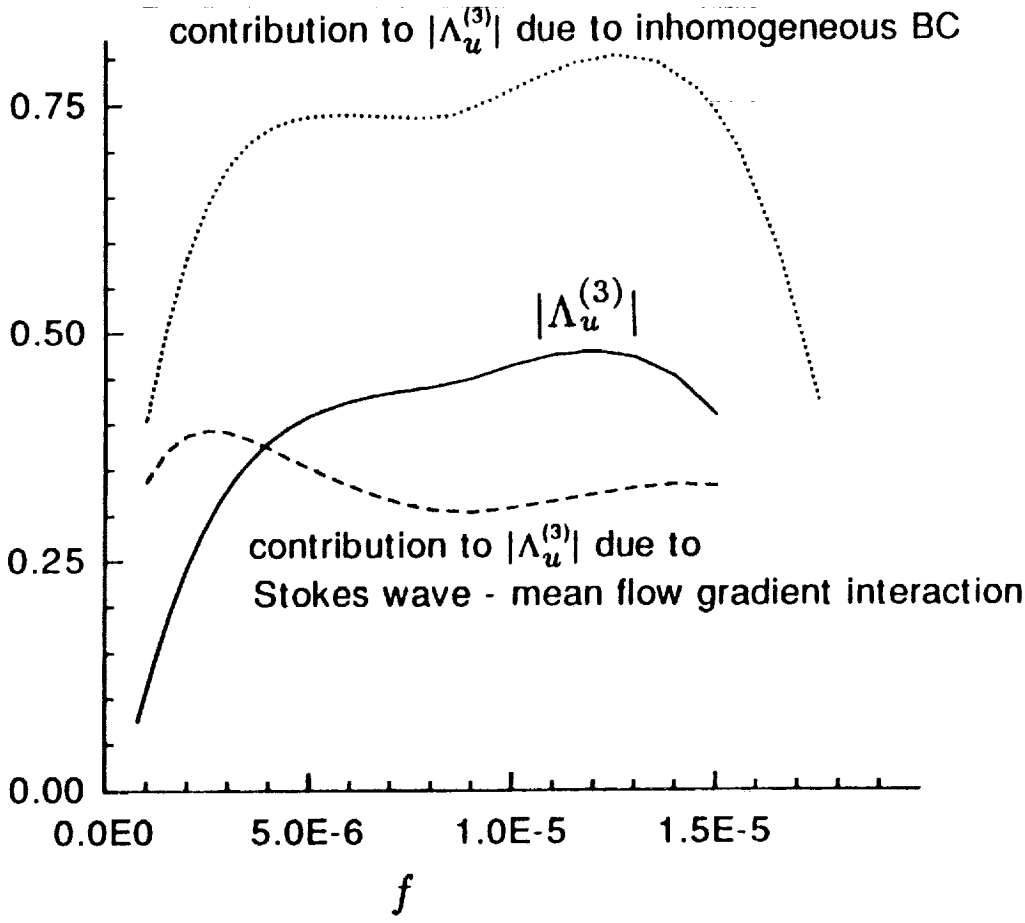

Fig. 8 Relative contributions of the source term in the differential equation, (2.13), and the inhomogeneous boundary condition, (2.16b), to $|\Lambda_u^{(3)}|$ for the case of receptivity due to wall hump located at $R = 2800$.

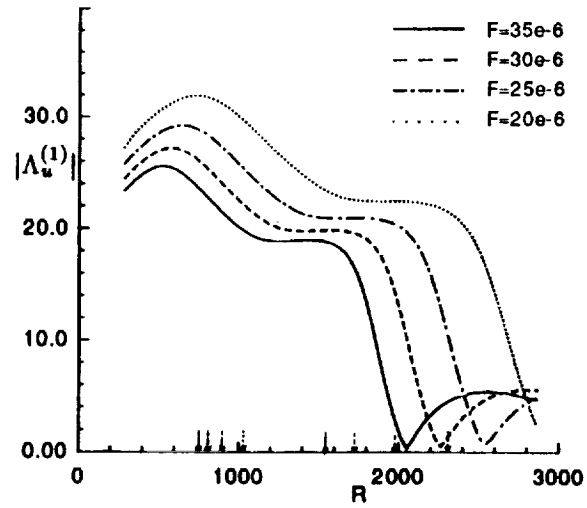

(a) Receptivity due to wall suction variation

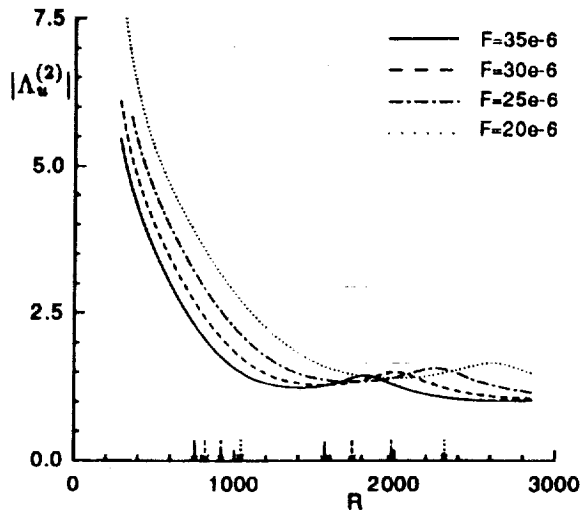

(b) Receptivity due to wall admittance variation

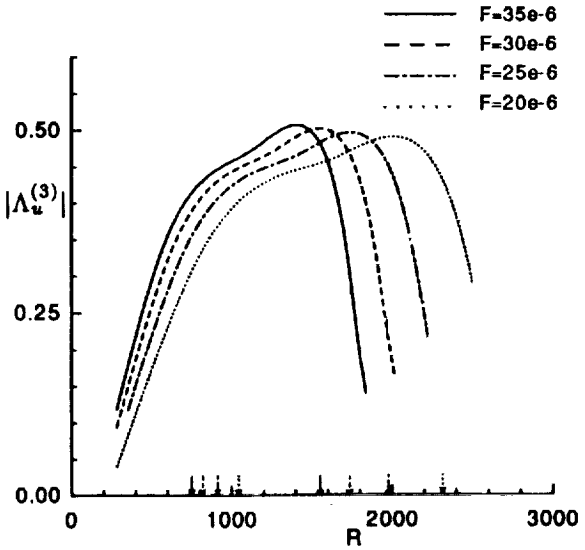

(c) Receptivity due to wall geometry variation

Fig. 9 Magnitudes of the efficiency functions $\Lambda_u^{(j)}, j = 1 - 3$ from Eq. (2.20b) as functions of the wall inhomogeneity location ($R \equiv \sqrt{Re_{\ell^*}} = R_{\delta^*}/1.72$) with $f = \omega^* \nu_\infty^* / {U_\infty^*}^2$ as a parameter.

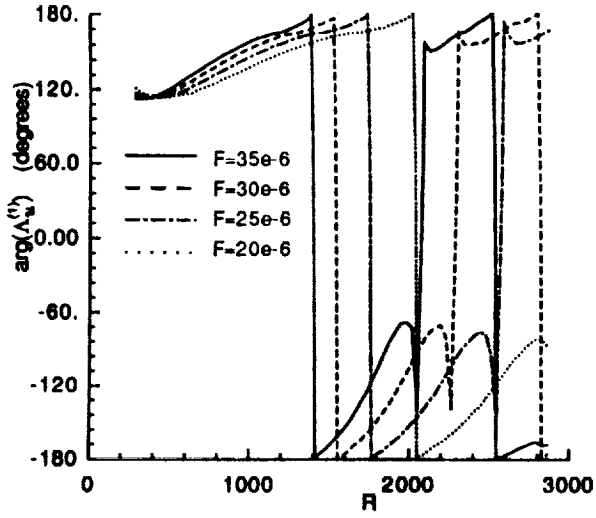

(a) Receptivity due to wall suction variation

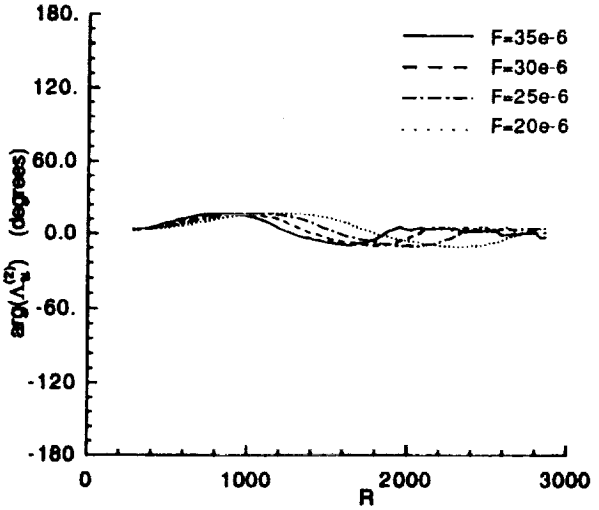

(b) Receptivity due to wall admittance variation

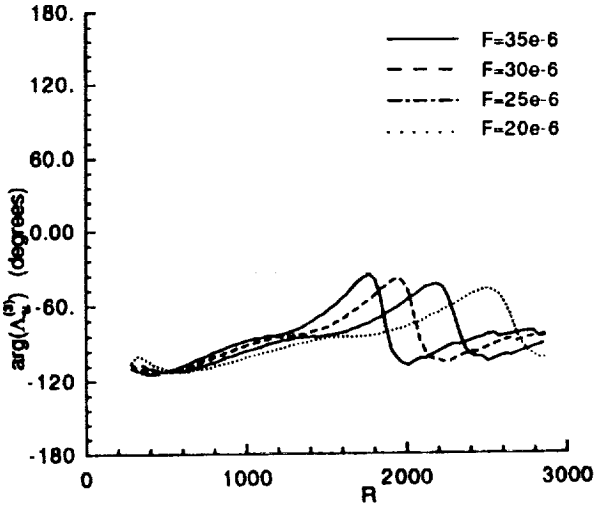

(c) Receptivity due to wall geometry variation

Fig. 10 Phase of the complex valued efficiency functions $\Lambda_u^{(j)}, j = 1 - 3$ from Eq. (2.20b) as functions of the wall inhomogeneity location ($R \equiv \sqrt{Re_{\ell^*}} = R_{\delta^*}/1.72$) with $f = \omega^* \nu_\infty^* / {U_\infty^*}^2$ as a parameter.

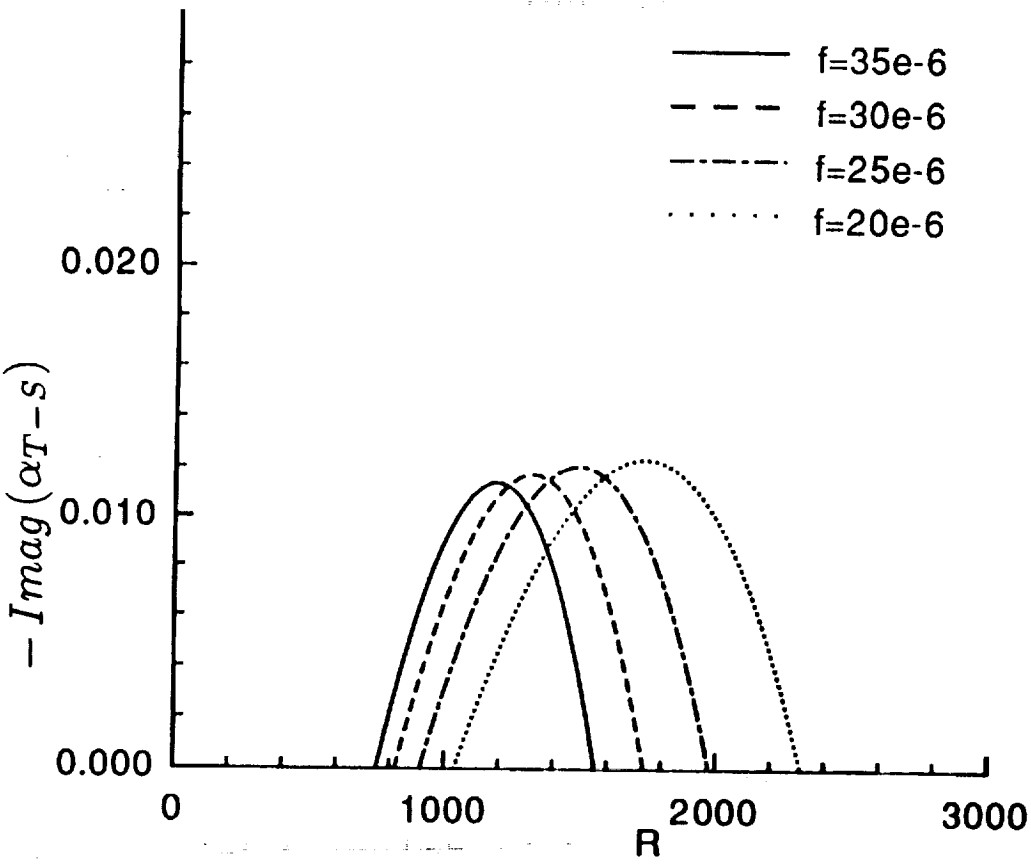

Fig. 11 Streamwise growth rate, $-Imag(\alpha_{T-S})$, as a function of R for the same values of f as in Figs. 9 and 10.

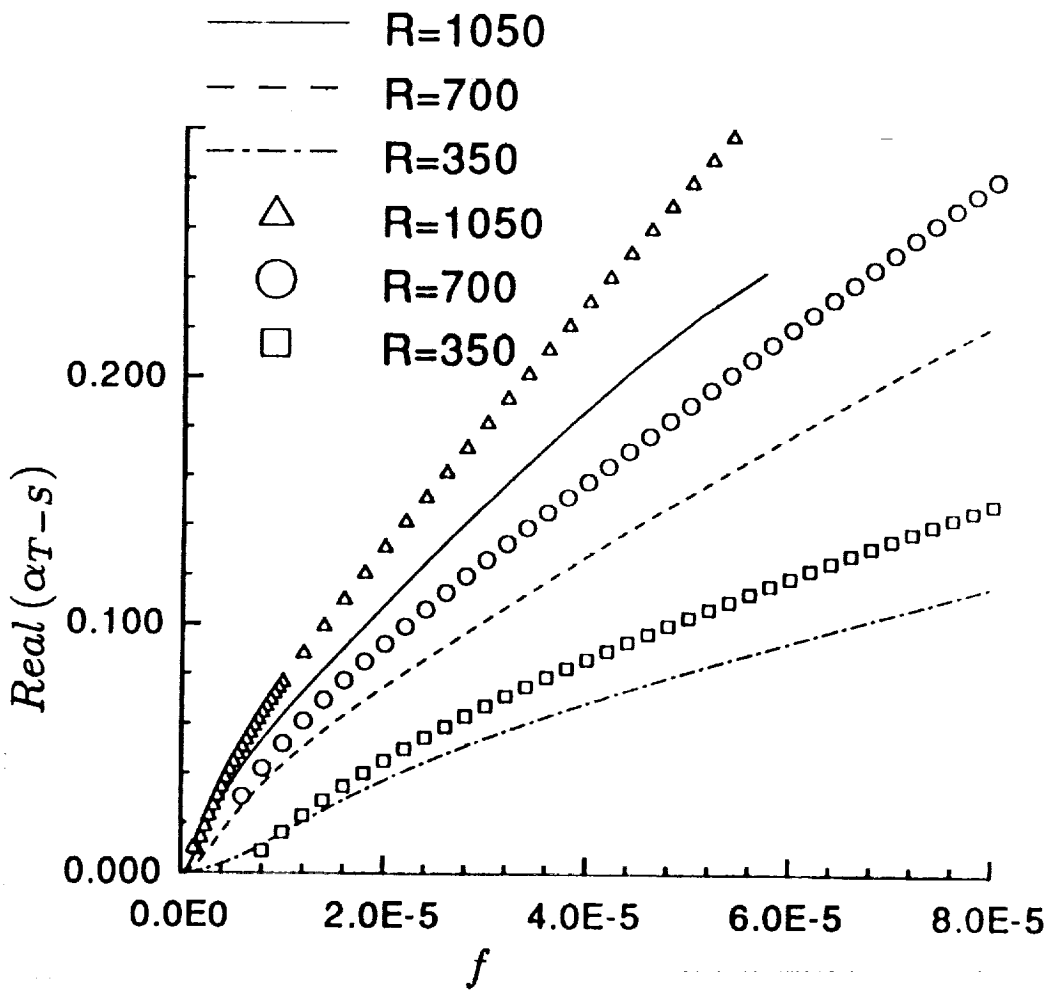

Fig. 12 Real part of the instability wavenumber, $Real\,(\alpha_{T-S})$, as a function of f in the range $R = 350$ to $R = 1050$.

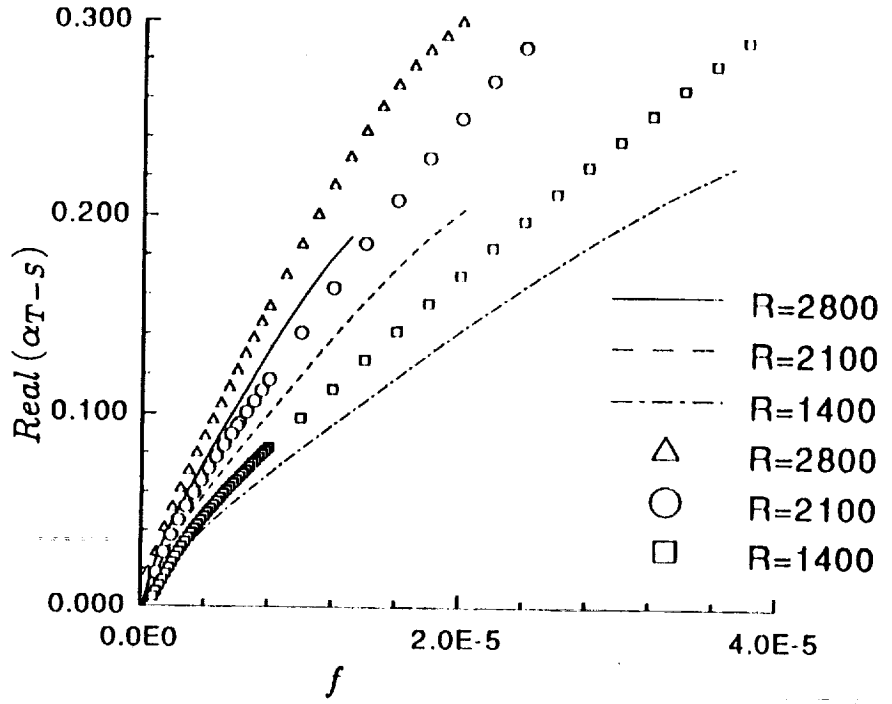

Fig. 13a Real part of the instability wavenumber, $Real\,(\alpha_{T-S})$, as a function of f in the range $R = 1400$ to $R = 2800$.

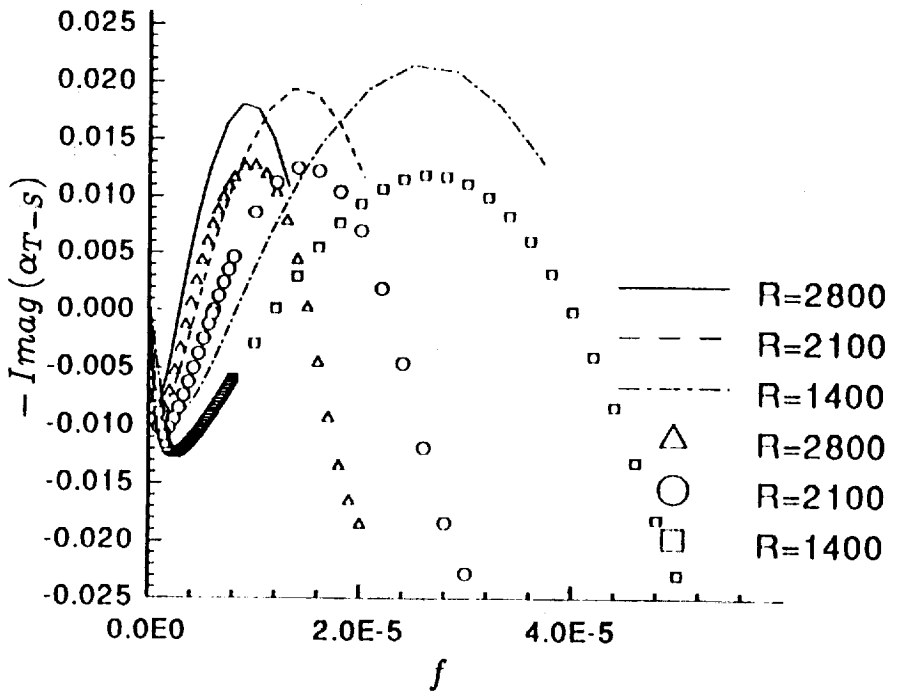

Fig. 13b Streamwise growth rate, $-Imag\,(\alpha_{T-S})$, as a function of f in the range $R = 1400$ to $R = 2800$.

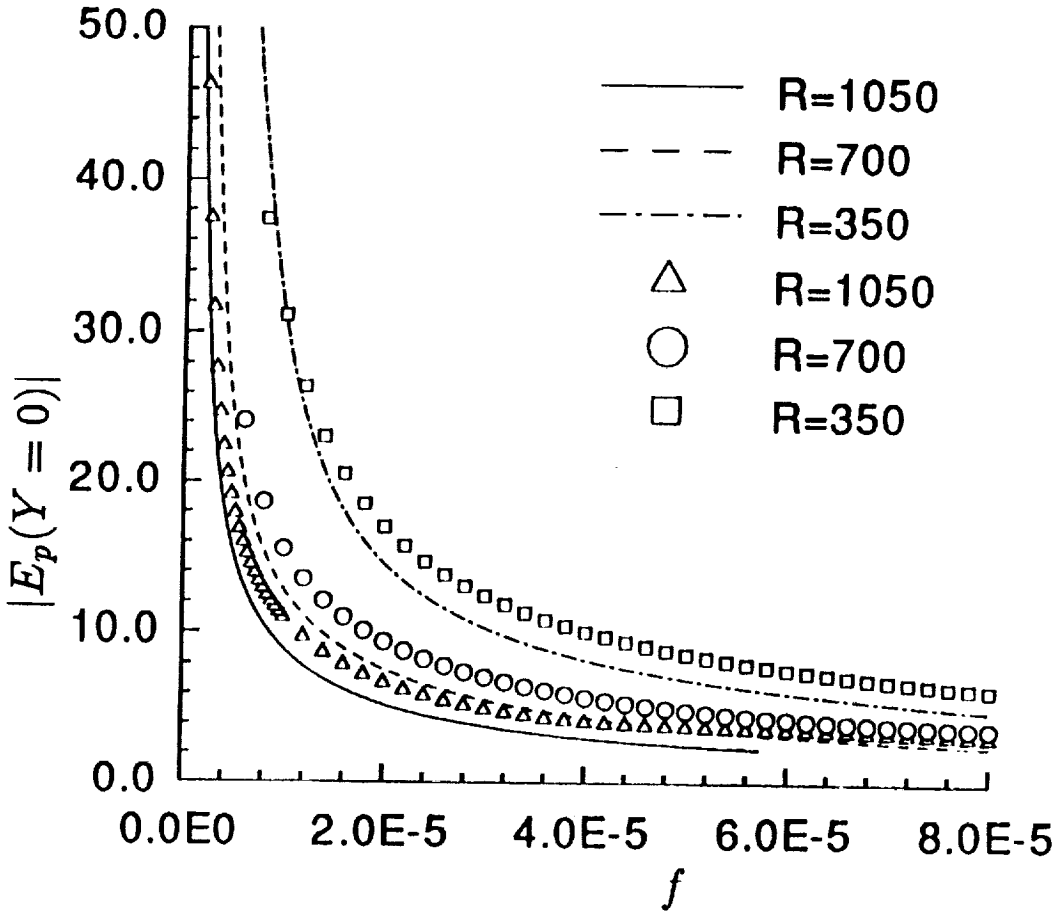

Fig. 14 Magnitude of the factor $E_p(Y = 0)$ from (2.21c), which relates the two types of efficiency functions, $\Lambda_u^{(j)}$ and $\Lambda_p^{(j)}$, plotted as a function of f for the same locations of the wall inhomogeneity as in Figs. 3a-3c.

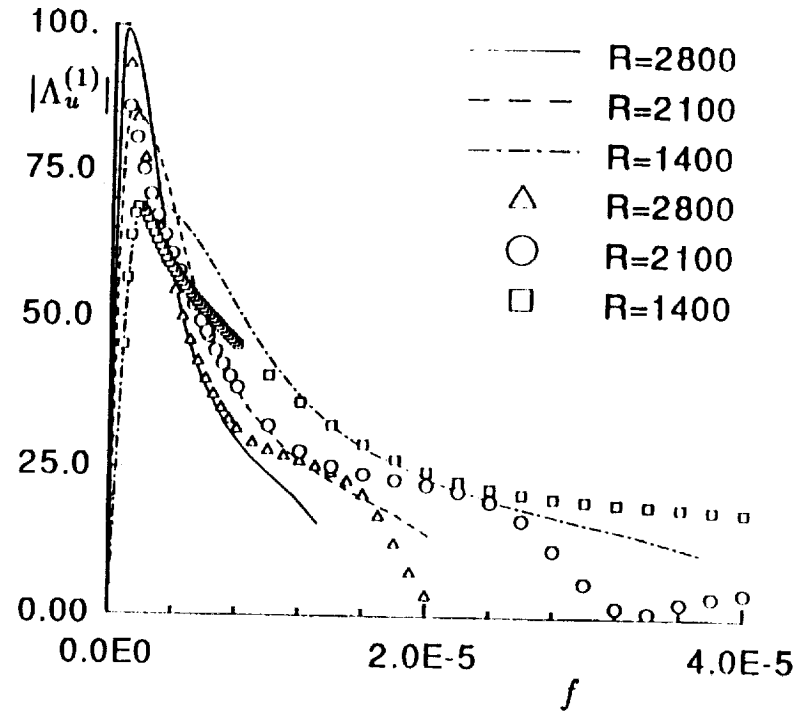

(a) Receptivity due to wall suction variation

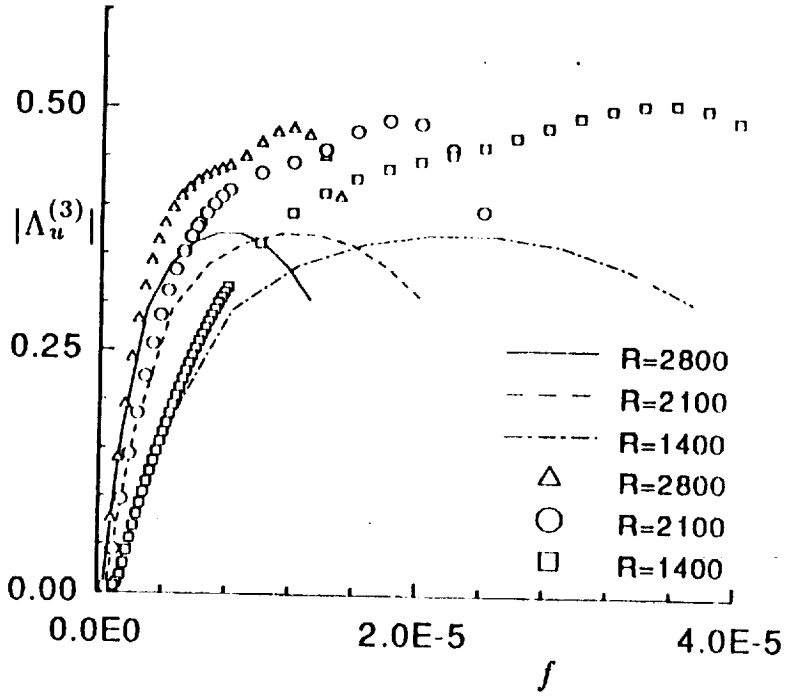

(b) Receptivity due to wall geometry variation

Fig. 15 Magnitudes of the efficiency functions $\Lambda_u^{(j)}, j = 1, 3$ from Eq. (2.20b) as functions of the non-dimensional frequency parameter $f = \omega^* \nu_\infty^* / U_\infty^{*2}$, in the range $R = 1400$ to $R = 2800$. The symbols denote the results from the finite Reynolds number approach, while the lines correspond to asymptotic predictions.

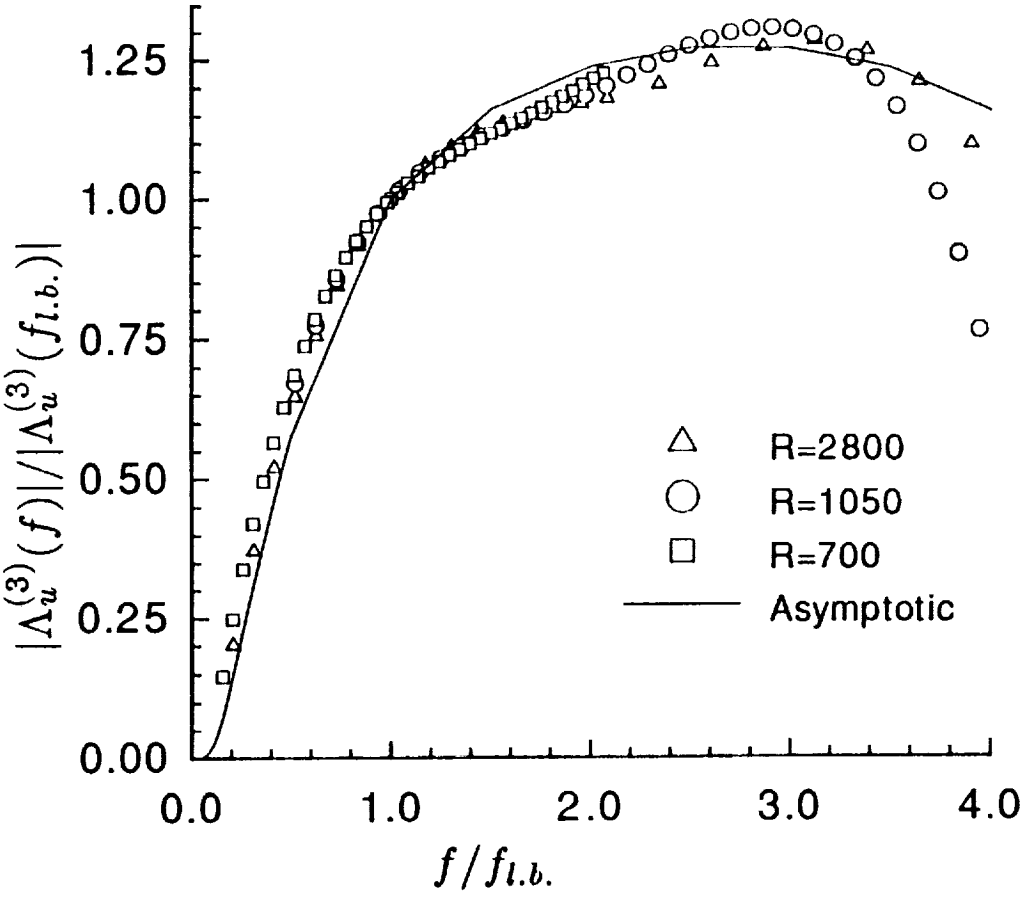

Fig. 16 Comparison of the numerical and asymptotic results for receptivity due to the wall hump : The normalized efficiency factor $|\Lambda_u^{(3)}(f)|/|\Lambda_u^{(3)}(f_{l.b.})|$ as a function of the normalized frequency parameter $f/f_{l.b.}$

Report Documentation Page

1. Report No.	2. Government Accession No.	3. Recipient's Catalog No.
NASA TM-102781		

4. Title and Subtitle	5. Report Date
A Finite Reynolds Number Approach for the Prediction of Boundary Layer Receptivity in Localized Regions	January 1991
	6. Performing Organization Code

7. Author(s)	8. Performing Organization Report No.
Meelan Choudhari Craig L. Streett	
	10. Work Unit No. 505-59-50-01
9. Performing Organization Name and Address	11. Contract or Grant No.
NASA Langley Research Center Hampton, Virginia 23665-5225	
	13. Type of Report and Period Covered Technical Memorandum
12. Sponsoring Agency Name and Address	14. Sponsoring Agency Code
National Aeronautics and Space Administration Washington, DC 20546-0001	

15. Supplementary Notes

Meelan Choudhari: High Technology Corp., Hampton, Virginia
Craig L. Streett: Langley Research Center, Hampton, Virginia

16. Abstract

Previous theoretical work on the boundary layer receptivity problem has utilized large Reynolds number asymptotic theories, thus being limited to a narrow part of the frequency - Reynolds number domain. We present an alternative approach for the prediction of localized instability generation which has a general applicability, and also accounts for finite Reynolds number effects. This approach is illustrated for the case of Tollmien-Schlichting wave generation in a Blasius boundary layer due to the interaction of a free-stream acoustic wave with a region of short-scale variation in the surface boundary condition. The specific types of wall inhomogeneities examined are: regions of short scale variations in wall suction, wall admittance and wall geometry (roughness). Extensive comparison is made between the results of the finite Reynolds number approach and previous asymptotic predictions, which also suggests an alternative way of utilizing the latter at Reynolds numbers of interest in practice.

17. Key Words (Suggested by Author(s))	18. Distribution Statement
Boundary Layer Receptivity Boundary Layer Transition Laminar Flow	Unclassified-Unlimited Subject Category: 02

19. Security Classif. (of this report)	20. Security Classif. (of this page)	21. No. of pages	22. Price
Unclassified	Unclassified	45	A03